

On identifying unobserved heterogeneity in stochastic blockmodel graphs with vertex covariates

Cong Mu, Angelo Mele, Lingxin Hao, Joshua Cape, Avanti Athreya, and Carey E. Priebe

Abstract—Both observed and unobserved vertex heterogeneity can influence block structure in graphs. To assess these effects on block recovery, we present a comparative analysis of two model-based spectral algorithms for clustering vertices in stochastic blockmodel graphs with vertex covariates. The first algorithm directly estimates the induced block assignments by investigating the estimated block connectivity probability matrix including the vertex covariate effect. The second algorithm estimates the vertex covariate effect and then estimates the induced block assignments after accounting for this effect. We employ Chernoff information to analytically compare the algorithms’ performance and derive the Chernoff ratio formula for some special models of interest. Analytic results and simulations suggest that, in general, the second algorithm is preferred: we can better estimate the induced block assignments by first estimating the vertex covariate effect. In addition, real data experiments on a diffusion MRI connectome data set indicate that the second algorithm has the advantages of revealing underlying block structure and taking observed vertex heterogeneity into account in real applications. Our findings emphasize the importance of distinguishing between observed and unobserved factors that can affect block structure in graphs.

Index Terms—Spectral graph inference, Chernoff ratio, stochastic blockmodel, vertex covariate.

I. INTRODUCTION

IN network inference applications, it is important to distinguish different factors such as vertex covariates and underlying vertex block assignments that can lead to networks with different latent communities. As a special case of random graph models, stochastic blockmodel (SBM) graphs are popular in the literature for community detection [1]–[3]. Inference in SBMs extended to include vertex covariates relies on either variational methods [4]–[6] or spectral approaches that promise applicability to large graphs [7]–[9]. Spectral methods [10] have been widely used in random graph models for a variety of subsequent inference tasks such as community detection [11]–[14], vertex nomination [15], nonparametric hypothesis testing [16], and multiple graph inference [17]. Two

particular spectral embedding methods, adjacency spectral embedding (ASE) and Laplacian spectral embedding (LSE), are popular since they enjoy nice properties including consistency [18] and asymptotic normality [19], [20]. To compare the performance of these two embedding methods, the concept of Chernoff information is first employed for SBMs [20] and then extended to consider the underlying graph structure [21].

One problem of interest in hypothesis testing framework is to assess the influence of unobserved vertex heterogeneity on outcome variables, controlling for vertex covariate effect [22], [23]. In a K -block SBM, that is to test whether $F_k = F$ for $k \in \{1, \dots, K\}$ given $\mathbf{y}_i | \tau_i = k \sim F_k$, where \mathbf{y}_i are outcome variables and τ_i is the induced block assignment for vertex i . To achieve this goal, it is crucial to estimate the block structure τ after accounting for the vertex covariate effect. Here we use “induced block assignment” to refer to the block assignment *after* accounting for the vertex covariate effect, since the number of blocks can change. An “induced” $K = 2$ SBM, but with each of the two blocks split into two via the effect of a binary vertex covariate, becomes a $K = 4$ SBM. We shall address this concept in detail in Section II.

In this article, we investigate two model-based spectral algorithms for clustering vertices in stochastic blockmodel graphs with vertex covariates. Analytically, we compare the algorithms’ performance via Chernoff information and derive the Chernoff ratio formula for special models of interest. We shall address the notion of Chernoff information for comparing algorithms in detail in Section IV. Practically, we compare the algorithms’ actual clustering performance by simulations and real data experiments on a diffusion MRI connectome data set.

The structure of this article is summarized as follows. Section II reviews relevant models for random graphs and the basic idea of spectral methods. Section III introduces our model-based spectral algorithms for clustering vertices in stochastic blockmodel graphs with vertex covariates. Section IV analytically compares the algorithms’ performance via Chernoff information and derives the Chernoff ratio formula for special models of interest. Section V provides simulations and real data experiments on a diffusion MRI connectome data set to compare the algorithms’ performance in terms of actual clustering performance. Section VI discusses the findings and presents some open questions for further investigation. Appendix A and Appendix B provide technical details for latent position geometry and analytic derivations of the Chernoff ratio.

Date of current version July 2, 2020.

This work was supported in part by the US National Science Foundation under Grant SES-1951005 and in part by the US Defense Advanced Research Projects Agency under the D3M program administered through contract FA8750-17-2-0112.

C. Mu, A. Athreya, and C.E. Priebe are with the Department of Applied Mathematics and Statistics, Johns Hopkins University, Baltimore, MD 21218. E-mail: {cmu2, dathrey1, cep}@jhu.edu.

A. Mele is with the Carey Business School, Johns Hopkins University, Baltimore, MD 21202. E-mail: angelo.mele@jhu.edu.

L. Hao is with the Department of Sociology, Johns Hopkins University, Baltimore, MD 21218. E-mail: hao@jhu.edu.

J. Cape is with the Department of Statistics, University of Pittsburgh, Pittsburgh, PA 15260. E-mail: joshua.cape@pitt.edu.

II. MODELS AND SPECTRAL METHODS

We consider the latent position model [24], [25] for edge-independent random graphs in which each vertex is associated with a latent position $\mathbf{X}_i \in \mathcal{X}$ where \mathcal{X} is some latent space such as \mathbb{R}^d , and edges between vertices arise independently with probability $\mathbf{P}_{ij} = \kappa(\mathbf{X}_i, \mathbf{X}_j)$ for some kernel function $\kappa : \mathcal{X} \times \mathcal{X} \rightarrow [0, 1]$. In particular, we focus on the generalized random dot product graph (GRDPG) where the kernel function is taken to be the (indefinite) inner product, which can include more flexible SBMs as special cases.

Definition 1 (Generalized Random Dot Product Graph [26]). Let $\mathbf{I}_{d_+d_-} = \mathbf{I}_{d_+} \oplus (-\mathbf{I}_{d_-})$ with $d_+ \geq 1$ and $d_- \geq 0$. Let F be a d -dimensional inner product distribution with $d = d_+ + d_-$ on $\mathcal{X} \subset \mathbb{R}^d$ satisfying $\mathbf{x}^\top \mathbf{I}_{d_+d_-} \mathbf{y} \in [0, 1]$ for all $\mathbf{x}, \mathbf{y} \in \mathcal{X}$. Let \mathbf{A} be an adjacency matrix and $\mathbf{X} = [\mathbf{X}_1, \dots, \mathbf{X}_n]^\top \in \mathbb{R}^{n \times d}$ where $\mathbf{X}_i \sim F$, i.i.d. for all $i \in \{1, \dots, n\}$. Then we say $(\mathbf{A}, \mathbf{X}) \sim \text{GRDPG}(n, F, d_+, d_-)$ if $\mathbf{A}_{ij} | \mathbf{X}_i, \mathbf{X}_j \sim \text{Bernoulli}(\mathbf{P}_{ij})$ where $\mathbf{P}_{ij} = \mathbf{X}_i^\top \mathbf{I}_{d_+d_-} \mathbf{X}_j$ for any $i, j \in \{1, \dots, n\}$.

As a special case of the GRDPG model, the SBM can be used to model block structure in edge-independent random graphs.

Definition 2 (K -block Stochastic Blockmodel Graph [2]). The K -block stochastic blockmodel (SBM) graph is an edge-independent random graph with each vertex belonging to one of K blocks. It can be parametrized by a block connectivity probability matrix $\mathbf{B} \in [0, 1]^{K \times K}$ and a nonnegative vector of block assignment probabilities $\boldsymbol{\pi} \in \mathbb{R}^K$ summing to unity. Let \mathbf{A} be an adjacency matrix and $\boldsymbol{\tau}$ be a vector of block assignments with $\tau_i = k$ if vertex i is in block k (occurring with probability π_k). We say $(\mathbf{A}, \boldsymbol{\tau}) \sim \text{SBM}(n, \mathbf{B}, \boldsymbol{\pi})$ if $\mathbf{A}_{ij} | \tau_i, \tau_j \sim \text{Bernoulli}(\mathbf{P}_{ij})$ where $\mathbf{P}_{ij} = \mathbf{B}_{\tau_i \tau_j}$ for any $i, j \in \{1, \dots, n\}$.

Let $(\mathbf{A}, \boldsymbol{\tau}) \sim \text{SBM}(n, \mathbf{B}, \boldsymbol{\pi})$ as in Definition 2 where $\mathbf{B} \in [0, 1]^{K \times K}$ with d_+ strictly positive eigenvalues and d_- strictly negative eigenvalues. To represent this SBM in the GRDPG model, we can choose $\boldsymbol{\nu}_1, \dots, \boldsymbol{\nu}_K \in \mathbb{R}^d$ where $d = d_+ + d_-$ such that $\boldsymbol{\nu}_k^\top \mathbf{I}_{d_+d_-} \boldsymbol{\nu}_\ell = \mathbf{B}_{k\ell}$ for all $k, \ell \in \{1, \dots, K\}$. For example, we can take $\boldsymbol{\nu} = \mathbf{U}_B |\mathbf{S}_B|^{1/2}$ where $\mathbf{B} = \mathbf{U}_B \mathbf{S}_B \mathbf{U}_B^\top$ is the spectral decomposition of \mathbf{B} after re-ordering. Then we have the latent position of vertex i as $\mathbf{X}_i = \boldsymbol{\nu}_k$ if $\tau_i = k$. As an illustration, consider the prototypical 2-block SBM with rank one block connectivity probability matrix \mathbf{B} where $\mathbf{B}_{11} = p^2, \mathbf{B}_{22} = q^2, \mathbf{B}_{12} = \mathbf{B}_{21} = pq$ with $0 < p < q < 1$. Let \mathbf{X}_i be the latent position of vertex i where $\mathbf{X}_i = \boldsymbol{\nu}_1 = p$ if $\tau_i = 1$ and $\mathbf{X}_i = \boldsymbol{\nu}_2 = q$ if $\tau_i = 2$. Then we can represent this SBM in the GRDPG model with latent positions $\boldsymbol{\nu} = [p \quad q]^\top$ as

$$\mathbf{B} = \boldsymbol{\nu} \boldsymbol{\nu}^\top = \begin{bmatrix} p^2 & pq \\ pq & q^2 \end{bmatrix}. \quad (1)$$

An extension of GRDPG taking vertex covariates into consideration is available.

Definition 3 (GRDPG with Vertex Covariates [9]). Consider GRDPG as in Definition 1. Let $\mathbf{Z} \in \mathbb{R}^{n \times r}$ denote observed vertex covariates. Then we say

$(\mathbf{A}, \mathbf{X}, \mathbf{Z}, \beta) \sim \text{GRDPG-Cov}(n, F, d_+, d_-, f, h)$ if $\mathbf{A}_{ij} | \mathbf{X}_i, \mathbf{X}_j, \mathbf{Z}_i, \mathbf{Z}_j \sim \text{Bernoulli}(\mathbf{P}_{ij})$ where $\mathbf{P}_{ij} = h(\mathbf{X}_i^\top \mathbf{I}_{d_+d_-} \mathbf{X}_j + \beta^\top f(\mathbf{Z}_i, \mathbf{Z}_j))$ for any $i, j \in \{1, \dots, n\}$ with link functions $f : \mathbb{R}^r \times \mathbb{R}^r \rightarrow \mathbb{R}^r$ and $h : \mathbb{R} \rightarrow [0, 1]$.

Remark 1. A special case of the model in Definition 3 is to use the indicator function as f and the identity function as h with one binary covariate. I.e. $\mathbf{P}_{ij} = \mathbf{X}_i^\top \mathbf{I}_{d_+d_-} \mathbf{X}_j + \beta \mathbf{1}\{\mathbf{Z}_i = \mathbf{Z}_j\}$ for any $i, j \in \{1, \dots, n\}$ or $\mathbf{P} = \mathbf{X} \mathbf{I}_{d_+d_-} \mathbf{X}^\top + \frac{1}{2} \beta (\mathbf{1} + \mathbf{Z} \mathbf{Z}^\top)$ with $\mathbf{Z} \in \{-1, 1\}^n$. In the case of an SBM, we have $\mathbf{P}_{ij} = \mathbf{B}_{\tau_i \tau_j} + \beta \mathbf{1}\{\mathbf{Z}_i = \mathbf{Z}_j\}$.

Example 1 (2-block Rank One Model with One Binary Covariate). As an illustration, consider the rank one matrix \mathbf{B} in Eq. (1) and the SBM model in Remark 1. Let $\mathbf{Z} \in \{-1, 1\}^n$ denote the observed binary covariate. Assume $0 < \beta < 1$ with $p^2 + \beta, q^2 + \beta, pq + \beta \in [0, 1]$. Then we have the block connectivity probability matrix with the vertex covariate effect as

$$\mathbf{B}_Z = \begin{bmatrix} p^2 + \beta & p^2 & pq + \beta & pq \\ p^2 & p^2 + \beta & pq & pq + \beta \\ pq + \beta & pq & q^2 + \beta & q^2 \\ pq & pq + \beta & q^2 & q^2 + \beta \end{bmatrix}. \quad (2)$$

Example 2 (2-block Homogeneous Model with One Binary Covariate). As a second illustration, consider the rank two matrix \mathbf{B} where $\mathbf{B}_{11} = \mathbf{B}_{22} = a, \mathbf{B}_{12} = \mathbf{B}_{21} = b$ with $0 < b < a < 1$. The SBMs parametrized by this \mathbf{B} lead to the notion of the homogeneous model [1], [21]. For K -block homogeneous model, we have $\mathbf{B}_{k\ell} = a$ for $k = \ell$ and $\mathbf{B}_{k\ell} = b$ for $k \neq \ell$. Assume $0 < \beta < 1$ with $a + \beta, b + \beta \in [0, 1]$. We then have the block connectivity probability matrix with the vertex covariate effect as

$$\mathbf{B}_Z = \begin{bmatrix} a + \beta & a & b + \beta & b \\ a & a + \beta & b & b + \beta \\ b + \beta & b & a + \beta & a \\ b & b + \beta & a & a + \beta \end{bmatrix}. \quad (3)$$

Note that in both of these examples, an induced 2-block SBM becomes a 4-block SBM via the effect of a binary vertex covariate. The goal is to cluster each vertex into one of the two induced blocks after accounting for the vertex covariate effect.

Definition 4 (Adjacency Spectral Embedding). Let $\mathbf{A} \in \{0, 1\}^{n \times n}$ be an adjacency matrix with eigendecomposition $\mathbf{A} = \sum_{i=1}^n \lambda_i \mathbf{u}_i \mathbf{u}_i^\top$ where $|\lambda_1| \geq \dots \geq |\lambda_n|$ are the magnitude-ordered eigenvalues and $\mathbf{u}_1, \dots, \mathbf{u}_n$ are the corresponding orthonormal eigenvectors. Given the embedding dimension $d < n$, the adjacency spectral embedding (ASE) of \mathbf{A} into \mathbb{R}^d is the $n \times d$ matrix $\tilde{\mathbf{X}} = \mathbf{U}_A |\mathbf{S}_A|^{1/2}$ where $\mathbf{S}_A = \text{diag}(\lambda_1, \dots, \lambda_d)$ and $\mathbf{U}_A = [\mathbf{u}_1 | \dots | \mathbf{u}_d]$.

Remark 2. There are different methods for choosing the embedding dimension [27], [28]; we adopt the simple and efficient profile likelihood method [29] to automatically identify “elbow”, which is the cut-off between the signal dimensions and the noise dimensions in scree plot.

In this article, we will focus on applying ASE for our inference task. The adaptation of our algorithms and analytic

derivations to the Laplacian spectral embedding can be a valuable future contribution.

III. MODEL-BASED SUBSEQUENT INFERENCE VIA SPECTRAL METHODS

We are interested in the inference task of estimating the induced block assignments in a SBM with vertex covariates. To that end, we also consider algorithms for estimating the vertex covariate effect, which can be further used to estimate the induced block assignments. For simplicity, we consider all algorithms with identity link and one binary covariate as in Remark 1. Generalization to the case with other link functions and more than one covariate can be a valuable future contribution.

Algorithm 1: Estimation of induced block assignment including the vertex covariate effect

Input: Adjacency matrix $\mathbf{A} \in \{0, 1\}^{n \times n}$

Output: Block assignments including the vertex covariate effect as $\hat{\xi}$; induced block assignments after accounting for the vertex covariate effect as $\hat{\tau}$.

- 1 Estimate latent positions including the vertex covariate effect as $\hat{\mathbf{Y}} \in \mathbb{R}^{n \times \hat{d}}$ using ASE of \mathbf{A} where \hat{d} is chosen as in Remark 2.
- 2 Cluster $\hat{\mathbf{Y}}$ using Gaussian mixture modeling (GMM) to estimate the block assignments including the vertex covariate effect as $\hat{\xi} \in \{1, \dots, \hat{K}\}^n$ where \hat{K} is chosen via Bayesian Information Criterion (BIC).
- 3 Compute the estimated block connectivity probability matrix including the vertex covariate effect as

$$\hat{\mathbf{B}}_Z = \hat{\boldsymbol{\mu}} \mathbf{I}_{\hat{d}_+ \hat{d}_-} \hat{\boldsymbol{\mu}}^\top \in [0, 1]^{\hat{K} \times \hat{K}},$$

where $\hat{\boldsymbol{\mu}} \in \mathbb{R}^{\hat{K} \times \hat{d}}$ is the estimated means of all clusters.

- 4 Cluster the diagonal of $\hat{\mathbf{B}}_Z$ using GMM to estimate the cluster assignments of the diagonal as $\hat{\phi} \in \{1, \dots, \frac{\hat{K}}{2}\}^{\hat{K}}$.
 - 5 Estimate the induced block assignments as $\hat{\tau}$ by $\hat{\tau}_k = c$ for $k \in \{i \mid \hat{\xi}_i = t \text{ for } t \in \{j \mid \hat{\phi}_j = c\}\}$ and $c = 1, \dots, \frac{\hat{K}}{2}$.
-

Note that in Algorithm 1, the estimation of the induced block assignments, i.e., $\hat{\tau}$, highly depends on the estimated block connectivity probability matrix $\hat{\mathbf{B}}_Z$. This suggests that we may not obtain an accurate estimate of the induced block assignments if $\hat{\mathbf{B}}_Z$ is not well-structured, which is often the case in real applications. Thus we propose a modified algorithm that will use additional information from vertex covariates to estimate the induced block assignments along with vertex covariate effect.

As an illustration of estimating β (Step 2 in Algorithm 2), consider the block connectivity probability matrix \mathbf{B}_Z as in Eq. (3). To get β , we can subtract two specific entries of \mathbf{B}_Z . For example,

Algorithm 2: Estimation of induced block assignment after accounting for the vertex covariate effect

Input: Adjacency matrix $\mathbf{A} \in \{0, 1\}^{n \times n}$; observed vertex covariates $\mathbf{Z} \in \{-1, 1\}^n$

Output: Block assignments including the vertex covariate effect as $\hat{\xi}$; induced block assignments after accounting for the vertex covariate effect as $\hat{\tau}$; estimated vertex covariate effect as $\hat{\beta}$.

- 1 1 - 4 in Algorithm 1.
- 2 Estimate the vertex covariate effect as $\hat{\beta}$ using one of the following procedures [9].
 - (a) Assign the block covariates as $\mathbf{Z}_B \in \{-1, 1\}^{\hat{K}}$ for each block using the mode, i.e.,

$$\mathbf{Z}_{B,k} = \begin{cases} -1 & \text{if } n_{-1,k} \geq n_{1,k} \\ 1 & \text{if } n_{-1,k} < n_{1,k} \end{cases},$$

where

$$n_{z,k} = \sum_{i: \hat{\xi}_i = k} \mathbf{1}\{\mathbf{Z}_i = z\}.$$

Construct pair set $S = \{(k\ell, k\ell'), k, \ell, \ell' \in \{1, \dots, \hat{K}\} \mid \hat{\phi}_\ell = \hat{\phi}_{\ell'}, \mathbf{Z}_{B,k} = \mathbf{Z}_{B,\ell}, \mathbf{Z}_{B,k} \neq \mathbf{Z}_{B,\ell'}\}$. Estimate the vertex covariate effect as

$$\hat{\beta}_{\text{SA}} = \frac{1}{|S|} \sum_{(k\ell, k\ell') \in S} \hat{\mathbf{B}}_{Z,k\ell} - \hat{\mathbf{B}}_{Z,k\ell'}.$$

(b) Compute the probability that two entries from $\hat{\mathbf{B}}_Z$ form a pair as

$$p_{k\ell, k\ell'} = \frac{n_{-1,k}n_{-1,\ell}n_{1,\ell'} + n_{1,k}n_{1,\ell}n_{-1,\ell'}}{n_k n_\ell n_{\ell'}},$$

where

$$n_k = \sum_{i=1}^n \mathbf{1}\{\hat{\xi}_i = k\}.$$

Construct pair set

$W = \{(\ell, \ell'), \ell, \ell' \in \{1, \dots, \hat{K}\} \mid \hat{\phi}_\ell = \hat{\phi}_{\ell'}\}$. Estimate the vertex covariate effect as

$$\hat{\beta}_{\text{WA}} = \frac{1}{\hat{K}|W|} \sum_{k=1}^{\hat{K}} \sum_{(\ell, \ell') \in W} p_{k\ell, k\ell'} (\hat{\mathbf{B}}_{Z,k\ell} - \hat{\mathbf{B}}_{Z,k\ell'}).$$

- 3 Account for the vertex covariate effect by

$$\tilde{\mathbf{A}}_{ij} = \mathbf{A}_{ij} - \hat{\beta} \mathbf{1}\{\mathbf{Z}_i = \mathbf{Z}_j\},$$

where $\hat{\beta}$ is either $\hat{\beta}_{\text{SA}}$ or $\hat{\beta}_{\text{WA}}$.

- 4 Estimate latent positions after accounting for the vertex covariate effect as $\tilde{\mathbf{Y}} \in \mathbb{R}^{n \times \tilde{d}}$ using ASE of $\tilde{\mathbf{A}}$ where \tilde{d} is chosen as in Remark 2.
 - 5 Cluster $\tilde{\mathbf{Y}}$ using GMM to estimate the induced block assignments after accounting for the vertex covariate effect as $\tilde{\tau} \in \{1, \dots, \frac{\hat{K}}{2}\}^n$.
-

$$\begin{aligned} \mathbf{B}_{Z,11} - \mathbf{B}_{Z,12} &= (a + \beta) - a = \beta, \\ \mathbf{B}_{Z,13} - \mathbf{B}_{Z,14} &= (b + \beta) - b = \beta. \end{aligned} \quad (4)$$

Then we can get $\hat{\beta}$ by subtracting two specific entries of $\hat{\mathbf{B}}_Z$. However, the ASE and GMM under GRDPG model can lead to the re-ordering of $\hat{\mathbf{B}}_Z$. Thus we need to identify pairs first so that we subtract the correct entries.

In Step 2(a), we find pairs in $\hat{\mathbf{B}}_Z$ by first assigning each block common covariates using the mode. However, it is possible that we can not find any pairs using this approach, especially in the unbalanced case where the size of each block is different and/or the distribution of the vertex covariate is different. For example, one block size is much larger than the others and/or vertex covariates are all the same within one block.

In Step 2(b), instead of first finding pairs using mode, we only compute the probability that two entries of $\hat{\mathbf{B}}_Z$ form a pair. This will make the estimation more robust to extreme cases or special structure.

IV. SPECTRAL INFERENCE PERFORMANCE

A. Chernoff Ratio

There are different metrics for comparing spectral inference performance such as within-class covariance and Chernoff information [3], [20], [30]. The within-class covariance will depend on which clustering procedure is used, specifically K -means. Chernoff information is independent of the clustering procedure and intrinsically related to the Bayes risk. We employ Chernoff information to compare the performance of Algorithm 1 and Algorithm 2 for estimating the induced block assignments in SBMs with vertex covariates. Let F_1 and F_2 be two continuous multivariate distributions on \mathbb{R}^d with density functions f_1 and f_2 . The Chernoff information [31], [32] is defined as

$$\begin{aligned} C(F_1, F_2) &= -\log \left[\inf_{t \in (0,1)} \int_{\mathbb{R}^d} f_1^t(\mathbf{x}) f_2^{1-t}(\mathbf{x}) d\mathbf{x} \right] \\ &= \sup_{t \in (0,1)} \left[-\log \int_{\mathbb{R}^d} f_1^t(\mathbf{x}) f_2^{1-t}(\mathbf{x}) d\mathbf{x} \right]. \end{aligned} \quad (5)$$

Consider the special case where we take $F_1 = \mathcal{N}(\boldsymbol{\mu}_1, \boldsymbol{\Sigma}_1)$ and $F_2 = \mathcal{N}(\boldsymbol{\mu}_2, \boldsymbol{\Sigma}_2)$; then the corresponding Chernoff information is

$$\begin{aligned} C(F_1, F_2) &= \sup_{t \in (0,1)} \left[\frac{1}{2} t(1-t) (\boldsymbol{\mu}_1 - \boldsymbol{\mu}_2)^\top \boldsymbol{\Sigma}_t^{-1} (\boldsymbol{\mu}_1 - \boldsymbol{\mu}_2) \right. \\ &\quad \left. + \frac{1}{2} \log \frac{|\boldsymbol{\Sigma}_t|}{|\boldsymbol{\Sigma}_1|^t |\boldsymbol{\Sigma}_2|^{1-t}} \right], \end{aligned} \quad (6)$$

where $\boldsymbol{\Sigma}_t = t\boldsymbol{\Sigma}_1 + (1-t)\boldsymbol{\Sigma}_2$. For a given embedding method such as ASE in Algorithm 1 and Algorithm 2, comparison via Chernoff information is based on the statistical information between the limiting distributions of the blocks and smaller statistical information implies less information to discriminate between different blocks of the SBM. To that end, we also

review the limiting results of ASE for SBM, essential for investigating Chernoff information.

Theorem 1 (CLT of ASE for SBM [26]). *Let $(\mathbf{A}^{(n)}, \mathbf{X}^{(n)}) \sim \text{GRDPG}(n, F, d_+, d_-)$ be a sequence of adjacency matrices and associated latent positions of a d -dimensional GRDPG as in Definition 1 from an inner product distribution F where F is a mixture of K point masses in \mathbb{R}^d , i.e.,*

$$F = \sum_{k=1}^K \pi_k \delta_{\boldsymbol{\nu}_k} \quad \text{with } \forall k, \pi_k > 0 \text{ and } \sum_{k=1}^K \pi_k = 1, \quad (7)$$

where $\delta_{\boldsymbol{\nu}_k}$ is the Dirac delta measure at $\boldsymbol{\nu}_k$. Let $\Phi(\mathbf{z}, \boldsymbol{\Sigma})$ denote the cumulative distribution function (CDF) of a multivariate Gaussian distribution with mean $\mathbf{0}$ and covariance matrix $\boldsymbol{\Sigma}$, evaluated at $\mathbf{z} \in \mathbb{R}^d$. Let $\hat{\mathbf{X}}^{(n)}$ be the ASE of $\mathbf{A}^{(n)}$ with $\hat{\mathbf{X}}_i^{(n)}$ as the i -th row (same for $\mathbf{X}_i^{(n)}$). Then there exists a sequence of matrices $\mathbf{M}_n \in \mathbb{R}^{d \times d}$ satisfying $\mathbf{M}_n \mathbf{I}_{d_+ d_-} \mathbf{M}_n^\top = \mathbf{I}_{d_+ d_-}$ such that for all $\mathbf{z} \in \mathbb{R}^d$ and fixed index i ,

$$\mathbb{P} \left\{ \sqrt{n} \left(\mathbf{M}_n \hat{\mathbf{X}}_i^{(n)} - \mathbf{X}_i^{(n)} \right) \leq \mathbf{z} \mid \mathbf{X}_i^{(n)} = \boldsymbol{\nu}_k \right\} \rightarrow \Phi(\mathbf{z}, \boldsymbol{\Sigma}_k), \quad (8)$$

where for $\boldsymbol{\nu} \sim F$

$$\begin{aligned} \boldsymbol{\Delta} &= \mathbb{E} [\boldsymbol{\nu} \boldsymbol{\nu}^\top], \\ \mathbb{E}_k &= \mathbb{E} [(\boldsymbol{\nu}_k^\top \mathbf{I}_{d_+ d_-} \boldsymbol{\nu}) (1 - \boldsymbol{\nu}_k^\top \mathbf{I}_{d_+ d_-} \boldsymbol{\nu}) \boldsymbol{\nu} \boldsymbol{\nu}^\top], \\ \boldsymbol{\Sigma}_k &= \mathbf{I}_{d_+ d_-} \boldsymbol{\Delta}^{-1} \mathbb{E}_k \boldsymbol{\Delta}^{-1} \mathbf{I}_{d_+ d_-}. \end{aligned} \quad (9)$$

Remark 3. If the adjacency matrix \mathbf{A} is sampled from an SBM parameterized by the block connectivity probability matrix \mathbf{B} in Eq. (1) and block assignment probabilities $\boldsymbol{\pi} = (\pi_1, \pi_2)$ with $\pi_1 + \pi_2 = 1$, then as a special case for Theorem 1 [20], [30], we have for each fixed index i ,

$$\begin{aligned} \sqrt{n} (\hat{X}_i - p) &\xrightarrow{d} \mathcal{N}(0, \sigma_p^2) \quad \text{if } X_i = p, \\ \sqrt{n} (\hat{X}_i - q) &\xrightarrow{d} \mathcal{N}(0, \sigma_q^2) \quad \text{if } X_i = q. \end{aligned} \quad (10)$$

where

$$\begin{aligned} \sigma_p^2 &= \frac{\pi_1 p^4 (1-p^2) + \pi_2 p q^3 (1-pq)}{[\pi_1 p^2 + \pi_2 q^2]^2}, \\ \sigma_q^2 &= \frac{\pi_1 p^3 q (1-pq) + \pi_2 q^4 (1-q^2)}{[\pi_1 p^2 + \pi_2 q^2]^2}. \end{aligned} \quad (11)$$

Now for a K -block SBM, let $\mathbf{B} \in [0, 1]^{K \times K}$ be the block connectivity probability matrix and $\boldsymbol{\pi} \in \mathbb{R}^K$ be the vector of block assignment probabilities. Given an n vertex instantiation of the SBM parameterized by \mathbf{B} and $\boldsymbol{\pi}$, for sufficiently large n , the large sample optimal error rate for estimating the block assignments using ASE can be measured via Chernoff information as [20], [30]

$$\begin{aligned} \rho &= \min_{k \neq \ell} \sup_{t \in (0,1)} \left[\frac{1}{2} n t(1-t) (\boldsymbol{\nu}_k - \boldsymbol{\nu}_\ell)^\top \boldsymbol{\Sigma}_{k\ell}^{-1}(t) (\boldsymbol{\nu}_k - \boldsymbol{\nu}_\ell) \right. \\ &\quad \left. + \frac{1}{2} \log \frac{|\boldsymbol{\Sigma}_{k\ell}(t)|}{|\boldsymbol{\Sigma}_k|^t |\boldsymbol{\Sigma}_\ell|^{1-t}} \right], \end{aligned} \quad (12)$$

where $\boldsymbol{\Sigma}_{k\ell}(t) = t\boldsymbol{\Sigma}_k + (1-t)\boldsymbol{\Sigma}_\ell$, $\boldsymbol{\Sigma}_k$ and $\boldsymbol{\Sigma}_\ell$ are defined as in Eq. (9). Also note that as $n \rightarrow \infty$, the logarithm term in

Eq. (12) will be dominated by the other term. Then we have the Chernoff ratio as

$$\rho^* = \frac{\rho_1^*}{\rho_2^*} \rightarrow \frac{\min_{k \neq \ell} \sup_{t \in (0,1)} \left[t(1-t)(\boldsymbol{\nu}_{1,k} - \boldsymbol{\nu}_{1,\ell})^\top \boldsymbol{\Sigma}_{1,k\ell}^{-1}(t)(\boldsymbol{\nu}_{1,k} - \boldsymbol{\nu}_{1,\ell}) \right]}{\min_{k \neq \ell} \sup_{t \in (0,1)} \left[t(1-t)(\boldsymbol{\nu}_{2,k} - \boldsymbol{\nu}_{2,\ell})^\top \boldsymbol{\Sigma}_{2,k\ell}^{-1}(t)(\boldsymbol{\nu}_{2,k} - \boldsymbol{\nu}_{2,\ell}) \right]}. \quad (13)$$

Here ρ_1^* and ρ_2^* are associated with the Algorithm 1 and Algorithm 2 respectively. If $\rho^* > 1$, then Algorithm 1 is preferred, otherwise Algorithm 2 is preferred.

B. 2-block Rank One Model with One Binary Covariate

As an illustration of using Chernoff ratio in Eq. (13) to compare the performance of Algorithm 1 and Algorithm 2 for estimating the induced block assignments, we consider the 2-block SBM with one binary covariate parametrized by the block connectivity probability matrix \mathbf{B}_Z as in Eq. (2). In addition, we consider the balanced case where $\boldsymbol{\pi} = (\frac{1}{2}, \frac{1}{2})$ and $\boldsymbol{\pi}_Z = (\frac{1}{4}, \frac{1}{4}, \frac{1}{4}, \frac{1}{4})$ with the assumption that $n_i = n\pi_i$ and $n_{Z,j} = n\pi_{Z,j}$ for $i \in \{1, 2\}$ and $j \in \{1, 2, 3, 4\}$. Via the idea of Cholesky decomposition, we can re-write \mathbf{B}_Z as

$$\mathbf{B}_Z = \boldsymbol{\nu}_Z \boldsymbol{\nu}_Z^\top = \begin{bmatrix} \boldsymbol{\nu}_1^\top \boldsymbol{\nu}_1 & \boldsymbol{\nu}_1^\top \boldsymbol{\nu}_2 & \boldsymbol{\nu}_1^\top \boldsymbol{\nu}_3 & \boldsymbol{\nu}_1^\top \boldsymbol{\nu}_4 \\ \boldsymbol{\nu}_2^\top \boldsymbol{\nu}_1 & \boldsymbol{\nu}_2^\top \boldsymbol{\nu}_2 & \boldsymbol{\nu}_2^\top \boldsymbol{\nu}_3 & \boldsymbol{\nu}_2^\top \boldsymbol{\nu}_4 \\ \boldsymbol{\nu}_3^\top \boldsymbol{\nu}_1 & \boldsymbol{\nu}_3^\top \boldsymbol{\nu}_2 & \boldsymbol{\nu}_3^\top \boldsymbol{\nu}_3 & \boldsymbol{\nu}_3^\top \boldsymbol{\nu}_4 \\ \boldsymbol{\nu}_4^\top \boldsymbol{\nu}_1 & \boldsymbol{\nu}_4^\top \boldsymbol{\nu}_2 & \boldsymbol{\nu}_4^\top \boldsymbol{\nu}_3 & \boldsymbol{\nu}_4^\top \boldsymbol{\nu}_4 \end{bmatrix}, \quad (14)$$

where $\boldsymbol{\nu}_Z = [\boldsymbol{\nu}_1 \ \boldsymbol{\nu}_2 \ \boldsymbol{\nu}_3 \ \boldsymbol{\nu}_4]^\top$. Elementary calculations yield the canonical latent positions as

$$\boldsymbol{\nu}_Z = \begin{bmatrix} \sqrt{p^2 + \beta} & 0 & 0 \\ \frac{p^2}{\sqrt{p^2 + \beta}} & \sqrt{\frac{\beta(2p^2 + \beta)}{p^2 + \beta}} & 0 \\ \frac{pq + \beta}{\sqrt{p^2 + \beta}} & \sqrt{\frac{\beta p^2(q-p)^2}{(p^2 + \beta)(2p^2 + \beta)}} & \sqrt{\frac{\beta(q-p)^2}{(2p^2 + \beta)}} \\ \frac{pq}{\sqrt{p^2 + \beta}} & \sqrt{\frac{\beta(p^2 + pq + \beta)^2}{(p^2 + \beta)(2p^2 + \beta)}} & \sqrt{\frac{\beta(q-p)^2}{(2p^2 + \beta)}} \end{bmatrix}. \quad (15)$$

For this model, the block connectivity probability matrix \mathbf{B}_Z as in Eq. (2) is positive semidefinite with $\text{rank}(\mathbf{B}_Z) = 3$. Then we have $\mathbf{I}_{d_+d_-} = \mathbf{I}_3$ and we can omit it in our analytic derivations. With the canonical latent positions in Eq. (15), the only remaining term to derive for Chernoff ratio is $\boldsymbol{\Sigma}_{k\ell}(t)$ in Eq. (13). For $t \in (0, 1)$, define

$$g_t(\boldsymbol{\nu}_k, \boldsymbol{\nu}_\ell, \boldsymbol{\nu}) = tg(\boldsymbol{\nu}_k, \boldsymbol{\nu}) + (1-t)g(\boldsymbol{\nu}_\ell, \boldsymbol{\nu}), \quad (16)$$

where

$$g(\boldsymbol{\nu}_k, \boldsymbol{\nu}) = (\boldsymbol{\nu}_k^\top \boldsymbol{\nu}) (1 - \boldsymbol{\nu}_k^\top \boldsymbol{\nu}). \quad (17)$$

Then we can re-write $\boldsymbol{\Sigma}_k$ in Eq. (9) as

$$\boldsymbol{\Sigma}_k = \boldsymbol{\Delta}^{-1} \mathbb{E} [g(\boldsymbol{\nu}_k, \boldsymbol{\nu}) \boldsymbol{\nu} \boldsymbol{\nu}^\top] \boldsymbol{\Delta}^{-1} \quad (18)$$

and $\boldsymbol{\Sigma}_{k\ell}(t)$ from Eq. (13) as

$$\boldsymbol{\Sigma}_{k\ell}(t) = \boldsymbol{\Delta}^{-1} \mathbb{E} [g_t(\boldsymbol{\nu}_k, \boldsymbol{\nu}_\ell, \boldsymbol{\nu}) \boldsymbol{\nu} \boldsymbol{\nu}^\top] \boldsymbol{\Delta}^{-1}. \quad (19)$$

To evaluate the Chernoff ratio, we also define for $1 \leq k < \ell \leq 4$

$$C_{k\ell} = \sup_{t \in (0,1)} t(1-t)(\boldsymbol{\nu}_k - \boldsymbol{\nu}_\ell)^\top \boldsymbol{\Sigma}_{k\ell}^{-1}(t)(\boldsymbol{\nu}_k - \boldsymbol{\nu}_\ell). \quad (20)$$

By the symmetric structure of \mathbf{B}_Z as in Eq. (2) and the balanced assumption, we observe that $C_{13} = C_{24}$, $C_{14} = C_{23}$. Thus we need only to evaluate C_{12} , C_{13} , C_{14} , C_{34} . Subsequent calculations and simplification yield

$$C_{12} = \frac{\beta^2}{2[\phi_p + \phi_{pq} + \beta(1 - p^2 - pq - \beta)]}, \quad (21)$$

$$C_{34} = \frac{\beta^2}{2[\phi_q + \phi_{pq} + \beta(1 - q^2 - pq - \beta)]},$$

where for $0 < p < q < 1$

$$\begin{aligned} \phi_p &= p^2(1 - p^2), \\ \phi_q &= q^2(1 - q^2), \\ \phi_{pq} &= pq(1 - pq). \end{aligned} \quad (22)$$

Then we have the approximate Chernoff information for Algorithm 1 as

$$\rho_1^* \approx \min_{k \in \{1,3\}, k < \ell \leq 4} C_{k\ell}, \quad (23)$$

where $C_{k\ell}$ for $k \in \{1, 3\}, k < \ell \leq 4$ are defined as in Eq. (21). For this model, there is no tractable closed-form for C_{13} and C_{14} but numerical experiments can be used to obtain ρ_1^* . By the Remark 3 and similar calculations [20], [30], we have the approximate Chernoff information for Algorithm 2 as

$$\begin{aligned} \rho_2^* &\approx \sup_{t \in (0,1)} t(1-t)(p-q)^2 [t\sigma_p^2 + (1-t)\sigma_q^2]^{-1} \\ &= \frac{(p-q)^2(p^2 + q^2)^2}{2[\sqrt{p^2\phi_p + q^2\phi_{pq}} + \sqrt{q^2\phi_q + p^2\phi_{pq}}]^2}, \end{aligned} \quad (24)$$

where σ_p^2, σ_q^2 are defined as in Eq. (11) and $\phi_p, \phi_q, \phi_{pq}$ are defined as in Eq. (22).

Figure 1 shows the Chernoff ratio when we fix $p = 0.3$ and take $q \in (0.3, 0.7), \beta \in (0.1, 0.5)$ in the 2-block rank one models with one binary covariate. We can see that $\rho^* < 1$ for most of the region while $\rho^* > 1$ only when q and β are relatively large. Recall that the performance of Algorithm 1 highly depends on the estimated block connectivity probability matrix $\hat{\mathbf{B}}_Z$. Large q and β lead to a relatively well-structured $\hat{\mathbf{B}}_Z$ and thus Algorithm 1 can have better performance in this region.

C. 2-block Homogeneous Model with One Binary Covariate

Now we consider the 2-block SBM with one binary covariate parametrized by the block connectivity probability matrix \mathbf{B}_Z as in Eq. (3). We also consider the balanced case where $\boldsymbol{\pi} = (\frac{1}{2}, \frac{1}{2})$ and $\boldsymbol{\pi}_Z = (\frac{1}{4}, \frac{1}{4}, \frac{1}{4}, \frac{1}{4})$ with the assumption that $n_i = n\pi_i$ and $n_{Z,j} = n\pi_{Z,j}$ for $i \in \{1, 2\}$ and $j \in \{1, 2, 3, 4\}$.

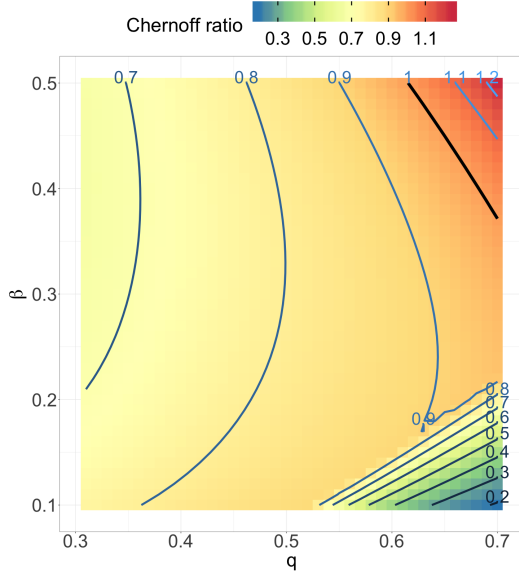


Fig. 1. Chernoff ratio as in Eq. (13) for 2-block rank one model, $p = 0.3, q \in (0.3, 0.7)$, $\beta \in (0.1, 0.5)$, $\pi = (\frac{1}{2}, \frac{1}{2})$, $\pi_Z = (\frac{1}{4}, \frac{1}{4}, \frac{1}{4}, \frac{1}{4})$.

Similarly, the idea of Cholesky decomposition and elementary calculations yield the canonical latent positions as

$$\nu_Z = \begin{bmatrix} \sqrt{a+\beta} & 0 & 0 \\ \frac{a}{\sqrt{a+\beta}} & \sqrt{\frac{\beta(2a+\beta)}{a+\beta}} & 0 \\ \frac{b+\beta}{\sqrt{a+\beta}} & \sqrt{\frac{\beta(b-a)^2}{(a+\beta)(2a+\beta)}} & \sqrt{\frac{2(a-b)(a+b+\beta)}{(2a+\beta)}} \\ \frac{b}{\sqrt{a+\beta}} & \sqrt{\frac{\beta(a+b+\beta)^2}{(a+\beta)(2a+\beta)}} & \sqrt{\frac{2(a-b)(a+b+\beta)}{(2a+\beta)}} \end{bmatrix}. \quad (25)$$

Observe that for this model, the block connectivity probability matrix \mathbf{B}_Z as in Eq. (3) is also positive semidefinite with $\text{rank}(\mathbf{B}_Z) = 3$. Then we have $\mathbf{I}_{d_+d_-} = \mathbf{I}_3$ and we can omit it in the derivations as for 2-block rank one model. To evaluate the Chernoff ratio, we also investigate the $C_{k\ell}$ as defined in Eq. (20). Similar observations suggest that $C_{12} = C_{34}, C_{13} = C_{24}, C_{14} = C_{23}$. Thus we only need to evaluate C_{12}, C_{13}, C_{14} . Subsequent calculations and simplification yield

$$\begin{aligned} C_{12} &= \frac{\beta^2}{2(\phi_a + \phi_b + \phi_\beta)}, \\ C_{13} &= \frac{(a-b)^2}{2(\phi_a + \phi_b + \phi_\beta)}, \\ C_{14} &= \frac{\beta^2 N_1 + (a-b)N_2}{2[D_1 + (\phi_a + \phi_b)(\phi_a + \phi_b + 2\phi_\beta)]}, \end{aligned} \quad (26)$$

where for $0 < b < a < 1$ and $0 < \beta < 1$

$$\begin{aligned} \phi_a &= a(1-a), \\ \phi_b &= b(1-b), \\ \phi_\beta &= \beta(1-a-b-\beta), \\ N_1 &= a(1-b) + b(1-a) + \phi_\beta \\ N_2 &= ab(a-b) + \phi_a(a+\beta) - \phi_b(b+\beta) \\ D_1 &= \beta^2(1-2a-\beta)(1-2b-\beta). \end{aligned} \quad (27)$$

Then we have the approximate Chernoff information for Algorithm 1 as

$$\rho_1^* \approx \min_{\ell \in \{2,3,4\}} C_{1\ell}, \quad (28)$$

where $C_{1\ell}$ for $\ell \in \{2,3,4\}$ are defined as in Eq. (26). Also observe that

$$\begin{aligned} C_{12} - C_{14} &= \frac{-(a-b)^2[\phi_a + \phi_b + \beta(1-a-b)]^2}{D_2}, \\ C_{13} - C_{14} &= \frac{-\beta^2 N_1^2}{D_2}, \end{aligned} \quad (29)$$

where

$$D_2 = 2(\phi_a + \phi_b + \phi_\beta)[D_1 + (\phi_a + \phi_b)(\phi_a + \phi_b + 2\phi_\beta)]. \quad (30)$$

Then we can further simplify ρ_1^* as

$$\rho_1^* \approx \begin{cases} \frac{\beta^2}{2(\phi_a + \phi_b + \phi_\beta)} & \text{if } \beta \leq a-b \\ \frac{(a-b)^2}{2(\phi_a + \phi_b + \phi_\beta)} & \text{if } \beta > a-b \end{cases}. \quad (31)$$

By the same derivations [21], we have the approximate Chernoff information for Algorithm 2 as

$$\rho_2^* \approx \frac{(a-b)^2}{2[a(1-a) + b(1-b)]} = \frac{(a-b)^2}{2(\phi_a + \phi_b)}, \quad (32)$$

where ϕ_a and ϕ_b are defined as in Eq. (27). We then have the general Chernoff ratio formula as follows.

Corollary 1. For 2-block homogeneous balanced model with one binary covariate parametrized by \mathbf{B}_Z as in Eq. (3) and $\pi_Z = (\frac{1}{4}, \frac{1}{4}, \frac{1}{4}, \frac{1}{4})$, the Chernoff ratio as in Eq. (13) can be derived analytically as

$$\rho^* = \frac{\rho_1^*}{\rho_2^*} \rightarrow \begin{cases} \frac{\beta^2(\phi_a + \phi_b)}{(a-b)^2(\phi_a + \phi_b + \phi_\beta)} & \text{if } \beta \leq a-b \\ \frac{\phi_a + \phi_b}{\phi_a + \phi_b + \phi_\beta} & \text{if } \beta > a-b \end{cases}, \quad (33)$$

where $\phi_a, \phi_b, \phi_\beta$ are defined as in Eq. (27).

Figure 2 shows Chernoff ratio when we fix $b = 0.1$ and take $a \in (0.1, 0.5), \beta \in (0.1, 0.5)$ in the 2-block homogeneous models with one binary covariate. Again we can see that $\rho^* < 1$ for most of the region while $\rho^* > 1$ only when a and β are relatively large, which agrees with the general formula for Chernoff ratio as in Corollary 1. According to Eq. (33), we can have $\rho^* > 1$ only when $\phi_\beta < 0$ and this can happen only when a and β are relatively large. This implies that, in general, Algorithm 2 is preferred for estimating the induced block assignments.

D. K-block Homogeneous Model with One Binary Covariate

We extend the discussion from the 2-block homogeneous model to the K -block homogeneous model with one binary covariate. Still, we consider the balanced case where $\pi = (\frac{1}{K}, \dots, \frac{1}{K})$ and $\pi_Z = (\frac{1}{2K}, \dots, \frac{1}{2K})$ with the assumption that $n_i = n\pi_i$ and $n_{Z,j} = n\pi_{Z,j}$ for $i \in \{1, \dots, K\}$ and $j \in \{1, \dots, 2K\}$. Similar observation and derivations yield

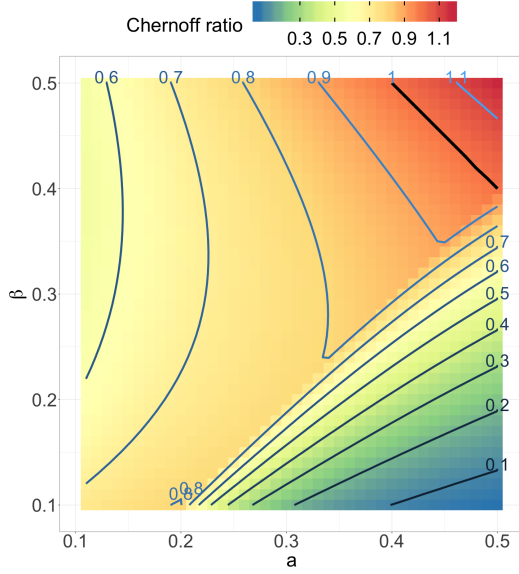


Fig. 2. Chernoff ratio as in Eq. (13) for 2-block homogeneous models. $b = 0.1, a \in (0.1, 0.5), \beta \in (0.1, 0.5), \pi = (\frac{1}{2}, \frac{1}{2}), \pi_Z = (\frac{1}{4}, \frac{1}{4}, \frac{1}{4}, \frac{1}{4})$.

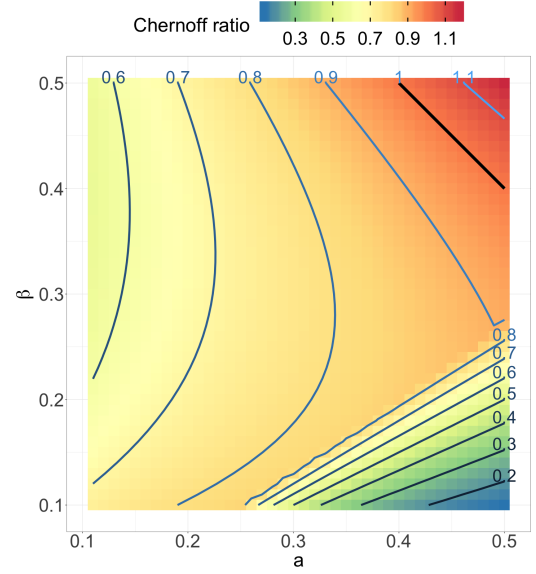


Fig. 3. Chernoff ratio as in Eq. (13) for 4-block homogeneous models. $b = 0.1, a \in (0.1, 0.5), \beta \in (0.1, 0.5), \pi = (\frac{1}{4}, \frac{1}{4}, \frac{1}{4}, \frac{1}{4}), \pi_Z = (\frac{1}{8}, \dots, \frac{1}{8})$.

the approximate Chernoff information for Algorithm 1 as (see Appendix A and Appendix B for more details)

$$\rho_1^* \approx \begin{cases} \frac{K\beta^2}{2D_4} & \text{if } \delta \leq 0 \\ \frac{(a-b)^2}{K(\phi_a + \phi_b + \phi_\beta)} & \text{if } \delta > 0 \end{cases}, \quad (34)$$

where $\phi_a, \phi_b, \phi_\beta$ are defined as in Eq. (27) and

$$\begin{aligned} D_3 &= K - 2a - 2(K-1)b - K\beta, \\ D_4 &= 2\phi_a + 2(K-1)\phi_b + \beta D_3, \\ \delta &= K^2\beta^2(\phi_a + \phi_b + \phi_\beta) - 2(a-b)^2D_4. \end{aligned} \quad (35)$$

Again by the same derivations [21], we have the approximate Chernoff information for Algorithm 2 as

$$\rho_2^* \approx \frac{(a-b)^2}{K[a(1-a) + b(1-b)]} = \frac{(a-b)^2}{K(\phi_a + \phi_b)}, \quad (36)$$

where ϕ_a and ϕ_b are defined as in Eq. (27). We then have the general Chernoff ratio formula as follows.

Theorem 2. For K -block homogeneous balanced model with one binary covariate parametrized by $\mathbf{B}_Z \in [0, 1]^{2K \times 2K}$ with similar structure as in Eq. (3) and $\pi_Z = (\frac{1}{2K}, \dots, \frac{1}{2K})$, the Chernoff ratio as in Eq. (13) can be derived analytically as

$$\rho^* = \frac{\rho_1^*}{\rho_2^*} \rightarrow \begin{cases} \frac{K^2\beta^2(\phi_a + \phi_b)}{2(a-b)^2D_4} & \text{if } \delta \leq 0 \\ \frac{\phi_a + \phi_b}{\phi_a + \phi_b + \phi_\beta} & \text{if } \delta > 0 \end{cases}, \quad (37)$$

where $\phi_a, \phi_b, \phi_\beta$ are defined as in Eq. (27), D_4, δ are defined as in Eq. (35).

Remark 4. Clearly Theorem 2 generalizes Corollary 1 beyond $K = 2$.

Figure 3 shows Chernoff ratio when we fix $b = 0.1$ and take $a \in (0.1, 0.5), \beta \in (0.1, 0.5)$ in the 4-block homogeneous

models with one binary covariate. We can see that $\rho^* < 1$ for most of the region while $\rho^* > 1$ only when a and β are relatively large. This implies again that, in general, Algorithm 2 is preferred for estimating the induced block assignments.

V. SIMULATIONS AND REAL DATA EXPERIMENTS

In addition to measuring the two algorithms' performance analytically via Chernoff ratio, we also compare Algorithm 1 and Algorithm 2 (with β and $\hat{\beta}$ in Step 3 respectively) by actual clustering results. Recall that the analytic comparison via Chernoff ratio is based on the limiting results of ASE for SBM when the number of vertices $n \rightarrow \infty$. The comparison via actual clustering results can measure the performance of these two algorithms for finite n .

As an illustration of this correspondence, we start with the setting related to "A" ($p = 0.3, q = 0.668, \beta = 0.49$ with $\rho^* = 1.1 > 1$) and "B" ($p = 0.3, q = 0.564, \beta = 0.49$ with $\rho^* = 0.91 < 1$) in left panel of Figure 4 for 2-block rank one model with one binary covariate $\mathbf{Z} \in \{1, 2\}^n$. We consider the balanced case where $n_1 = n_2 = \frac{n}{2}$ and $n_{Z,1} = n_{Z,2} = n_{Z,3} = n_{Z,4} = \frac{n}{4}$. For each $n \in \{100, 140, 180, 220, 260\}$, we simulate 100 adjacency matrices with $\frac{n}{2}$ vertices in each block and generate binary covariate with $\frac{n}{4}$ vertices having each value of \mathbf{Z} within each block. We then apply Algorithm 1 and Algorithm 2 (with β and $\hat{\beta}$ in Step 3 respectively) using embedding dimension $\hat{d} = 3$ to estimate the induced block assignments where adjusted Rand index (ARI) is used to measure the performance. The upper right panel in Figure 4 shows that although $\rho^* > 1$ and Algorithm 1 should be preferred in terms of Chernoff ratio, the ARI suggests that Algorithm 2 is preferred. Chernoff ratio is a limiting result. However, the region for which $\rho^* > 1$ is so easy for clustering—e.g., $q - p$ is large for "A"—that both algorithms are essentially perfect even for small n . The lower right panel in Figure 4

shows that Algorithm 2 tends to have better performance than Algorithm 1, which agrees with the Chernoff ratio as in left figure where $\rho^* < 1$ and Algorithm 2 is preferred.

To further investigate the flexibility of our models and algorithms, we also extend the discussion from binary to categorical vertex covariate.

A. 2-block Rank One Model with One 5-categorical Covariate

Specifically, we first consider the 2-block rank one model with one 5-categorical covariate $\mathbf{Z} \in \{1, 2, 3, 4, 5\}^n$, i.e., we have the block connectivity probability matrix $\mathbf{B}_Z \in [0, 1]^{10 \times 10}$ with the similar structure as in Eq. (2).

We first fix $p = 0.3, \beta = 0.4$ and consider $q \in \{0.35, 0.375, 0.4, 0.425, 0.45\}$. For each q , we simulate 100 adjacency matrices with 1000 vertices in each block and generate 5-categorical covariate with 200 vertices having each value of \mathbf{Z} within each block. We then apply Algorithm 1 and Algorithm 2 (with β and $\hat{\beta}$ in Step 3 respectively) using embedding dimension $\hat{d} = 6$ to estimate the induced block assignments. Figure 5a shows that both algorithms estimate more accurate induced block assignments as the latent positions of two induced block move away from each other, i.e., two induced blocks tend to be more separate, and Algorithm 2 can have better performance than Algorithm 1.

Next we fix $p = 0.3, q = 0.375$ and consider $\beta \in \{0.1, 0.15, 0.2, 0.25, 0.3\}$. For each β , we simulate 100 adjacency matrices with 1000 vertices in each block and generate 5-categorical covariate with 200 vertices having each value of \mathbf{Z} within each block. We then apply both algorithms (with β and $\hat{\beta}$ in Step 3 of Algorithm 2 respectively) using embedding dimension $\hat{d} = 6$ to estimate the induced block assignments. Figure 5b shows Algorithm 1 can only estimate accurate induced block assignments when β is relatively small while Algorithm 2 can estimate accurate induced block assignments no matter β is small or large. Intuitively, as Algorithm 1 directly estimates the induced block assignments, when β is relatively large, i.e., vertex covariates can affect block structure significantly, it lacks the ability to distinguish this effect. However, Algorithm 2 can use additional information from vertex covariates to estimate β , taking this effect into consideration when estimating the induced block assignments. Again, the overall performance of Algorithm 2 is better than that of Algorithm 1.

B. 2-block Homogeneous Model with One 5-categorical Covariate

We now consider the 2-block homogeneous model with one 5-categorical covariate $\mathbf{Z} \in \{1, 2, 3, 4, 5\}^n$, i.e., we have the block connectivity probability matrix $\mathbf{B}_Z \in [0, 1]^{10 \times 10}$ with the similar structure as in Eq. (3). Note that we can re-write \mathbf{B} like Eq. (1) as

$$\mathbf{B} = \boldsymbol{\nu} \boldsymbol{\nu}^\top = \begin{bmatrix} a & b \\ b & a \end{bmatrix} \quad \text{with } \boldsymbol{\nu} = \begin{bmatrix} \sqrt{a} & 0 \\ \frac{b}{\sqrt{a}} & \sqrt{\frac{(a-b)(a+b)}{a}} \end{bmatrix}. \quad (38)$$

With these canonical latent positions, the distance between two induced blocks can be measured by

$$\left(\sqrt{a} - \frac{b}{\sqrt{a}} \right)^2 + \left(0 - \sqrt{\frac{(a-b)(a+b)}{a}} \right)^2 = 2(a-b). \quad (39)$$

We first fix $b = 0.1, \beta = 0.2$ and consider $a \in \{0.12, 0.125, 0.13, 0.135, 0.14\}$. For each a , we simulate 100 adjacency matrices with 1000 vertices in each block and generate 5-categorical covariate with 200 vertices having each value of \mathbf{Z} within each block. We then apply both algorithms (with β and $\hat{\beta}$ in Step 3 of Algorithm 2 respectively) using embedding dimension $\hat{d} = 6$ to estimate the induced block assignments. Figure 6a shows that both algorithms estimate more accurate induced block assignments as the latent positions of two induced block move away from each other, i.e., two induced blocks tend to be more separate as measured by Eq. (39), and Algorithm 2 can have much better performance. Recall that Algorithm 1 tries to estimate the induced block assignments by clustering the diagonal of $\hat{\mathbf{B}}_Z$ and re-assigning the block assignments including the vertex covariate effect. For the homogeneous model, the diagonal of \mathbf{B}_Z are all the same, which can make it hard for Algorithm 1 to accurately estimate the induced block assignments. But Algorithm 2 is not affected by the homogeneous structure since it estimates the vertex covariate effect first and then estimates the induced block assignments by clustering the estimated latent positions like the canonical ones in Eq. (38).

Next we fix $a = 0.135, b = 0.1$ and consider $\beta \in \{-0.09, -0.08, -0.07, -0.06, -0.05\}$. For each β , we also simulate 100 adjacency matrices with 1000 vertices in each block and generate 5-categorical covariate with 200 vertices having each value of \mathbf{Z} within each block. We then apply both algorithms (with β and $\hat{\beta}$ in Step 3 of Algorithm 2 respectively) using embedding dimension $\hat{d} = 6$ to estimate the induced block assignments. Figure 6b shows that both algorithms are relative stable for this homogeneous model if we fix a and b , due to the special structure. Still, Algorithm 2 can have much better performance than Algorithm 1.

C. Connectome Data

We conduct real data experiments on a diffusion MRI connectome data set [33]. There are 114 graphs (connectomes) estimated by the NDMG pipeline [34] in this data set. Each vertex in these graphs has a {Left, Right} hemisphere label and a {Gray, White} tissue label.

We begin with a synthetic data analysis. We model the graphs as GRDPG with vertex covariates by applying two separate a priori 2-block projections as in [33]; in each case one label is treated as the induced block and the other label is treated as the binary vertex covariate. In particular, the a priori block connectivity probability matrices are given by

$$\mathbf{B}_{LR} = \begin{bmatrix} 0.050 & 0.013 \\ 0.013 & 0.051 \end{bmatrix} \quad \& \quad \mathbf{B}_{GW} = \begin{bmatrix} 0.011 & 0.027 \\ 0.027 & 0.079 \end{bmatrix}. \quad (40)$$

Furthermore, we have the block assignment probabilities from the data set as $\pi_{LR} = (0.5, 0.5), \pi_{GW} = (0.56, 0.44)$ and $\pi_{Z,LR} = (0.28, 0.22, 0.28, 0.22), \pi_{Z,GW} = (0.28, 0.28, 0.22, 0.22)$.

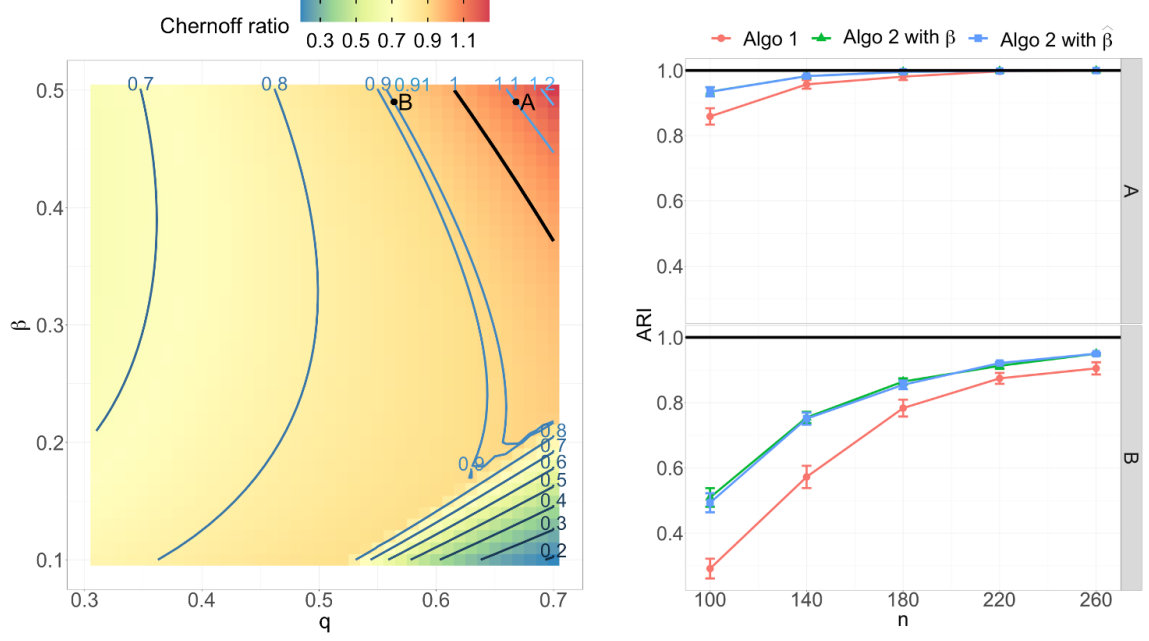


Fig. 4. Correspondence between Chernoff analysis and simulations.

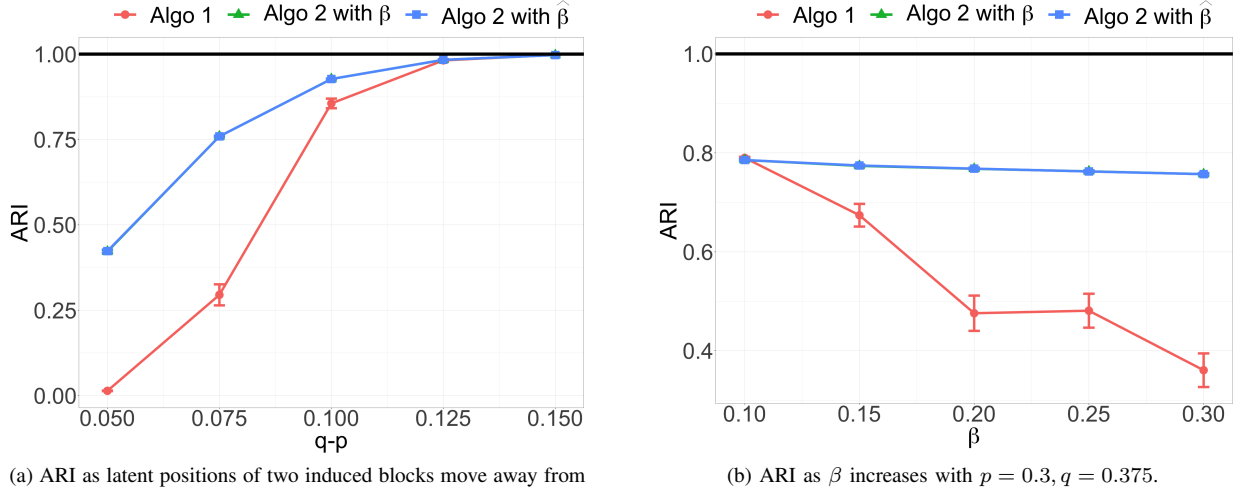


Fig. 5. Simulations for 2-block rank one model with one 5-categorical covariate, balanced case.

We first treat $\{\text{Left}, \text{Right}\}$ as the induced block and $\{\text{Gray}, \text{White}\}$ as the vertex covariate. For each $\beta \in \{0.050, 0.075, 0.100, 0.125, 0.150\}$, we simulate 100 adjacency matrices with $n = 1000$ where 280 vertices have label $\{\text{Left}\}$ and $\{\text{Gray}\}$, 220 vertices have label $\{\text{Left}\}$ and $\{\text{White}\}$, 280 vertices have label $\{\text{Right}\}$ and $\{\text{Gray}\}$, 220 vertices have label $\{\text{Right}\}$ and $\{\text{White}\}$. We then apply both algorithms (with β and $\hat{\beta}$ in Step 3 of Algorithm 2 respectively) using embedding dimension $\hat{d} = 3$ to estimate the induced block assignments. Figure 7a shows that Algorithm 2 can have much better performance than Algorithm 1. Note that \mathbf{B}_{LR} approximately has homogeneous structure; as discussed above, this diagonal structure can make it difficult for Algo-

rithm 1 to accurately estimate the induced block assignments while Algorithm 2 can first estimate the vertex covariate effect and then estimate the induced block assignments by clustering the latent positions after accounting for this effect.

We then treat $\{\text{Gray}, \text{White}\}$ as the induced block and $\{\text{Left}, \text{Right}\}$ as the vertex covariate. We fix $\beta = 0.03$ and consider $n \in \{400, 600, 800, 1000, 1200\}$. For each n , we simulate 100 adjacency matrices where $0.28n$ vertices have label $\{\text{Gray}\}$ and $\{\text{Left}\}$, $0.28n$ vertices have label $\{\text{Gray}\}$ and $\{\text{Right}\}$, $0.22n$ vertices have label $\{\text{White}\}$ and $\{\text{Left}\}$, $0.22n$ vertices have label $\{\text{White}\}$ and $\{\text{Right}\}$. We then apply both algorithms (with β and $\hat{\beta}$ in Step 3 of Algorithm 2 respectively) using embedding dimension $\hat{d} = 3$ to estimate

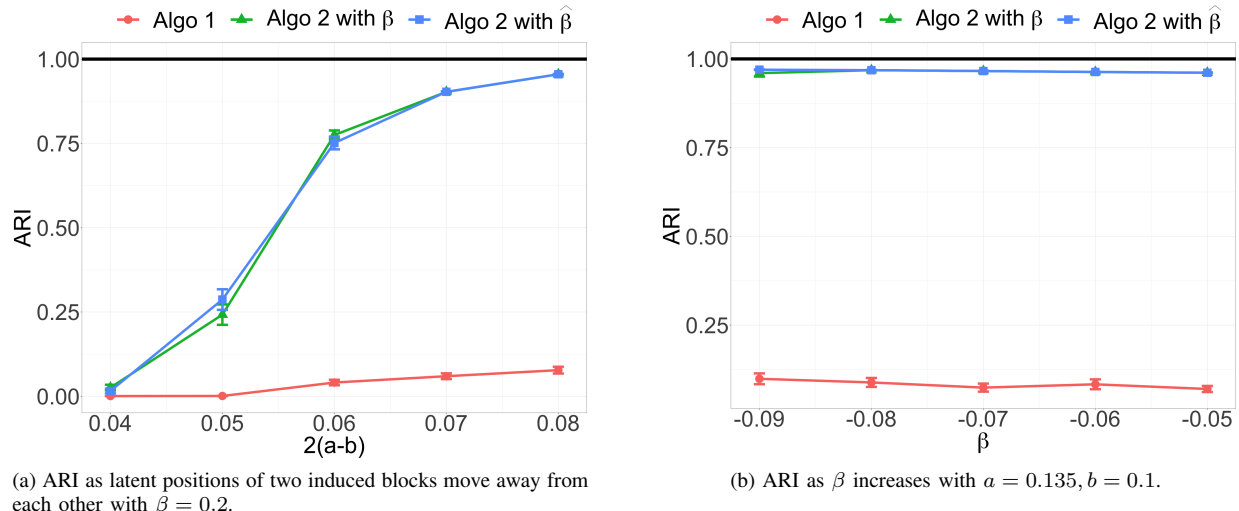


Fig. 6. Simulations for 2-block homogeneous model with one 5-categorical covariate, balanced case.

the induced block assignments. Figure 7b shows that both algorithms tend to have better performance as n increases and for small n Algorithm 2 again can have relatively better performance than Algorithm 1.

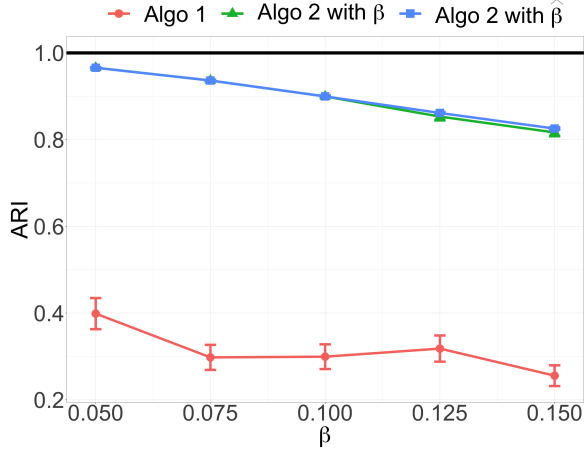
Now we apply our algorithms to the actual graphs from the connectome data set. Each of the 114 connectomes (the number of vertices $n \approx 40000$) is represented by a point in Figure 8 with $x = \text{ARI}(\text{Algo2, LR}) - \text{ARI}(\text{Algo1, LR})$ and $y = \text{ARI}(\text{Algo2, GW}) - \text{ARI}(\text{Algo1, GW})$ where $\text{ARI}(\text{Algo1, LR})$ denotes the ARI when we apply Algorithm 1 and treat $\{\text{Left, Right}\}$ as the induced block (with analogous notation for the rest). We see that most of the points lie in the $(+, +)$ quadrant, indicating $\text{ARI}(\text{Algo2, LR}) > \text{ARI}(\text{Algo1, LR})$ and $\text{ARI}(\text{Algo2, GW}) > \text{ARI}(\text{Algo1, GW})$. That is, Algorithm 2 is better at estimating the induced block assignments for this real application. Note that this claim holds no matter which label is treated as the induced block. This again emphasizes the importance of distinguishing different factors that can affect block structure in graphs. Algorithm 2 is able to identify particular block structure by using the observed vertex covariate information. That is, it is more likely to discover the $\{\text{Left, Right}\}$ structure after accounting for the effect of $\{\text{Gray, White}\}$ label and more likely to discover the $\{\text{Gray, White}\}$ structure after accounting for the effect of $\{\text{Left, Right}\}$ label. In real data, we may not have ground truth for the block structure. Our findings suggest that we are able to discover block structure by using observed vertex covariates, which can lead to meaningful insights in widely varying applications. That is, we can better reveal underlying block structure and thus better understand the data by accounting for the vertex covariate effect.

VI. DISCUSSION

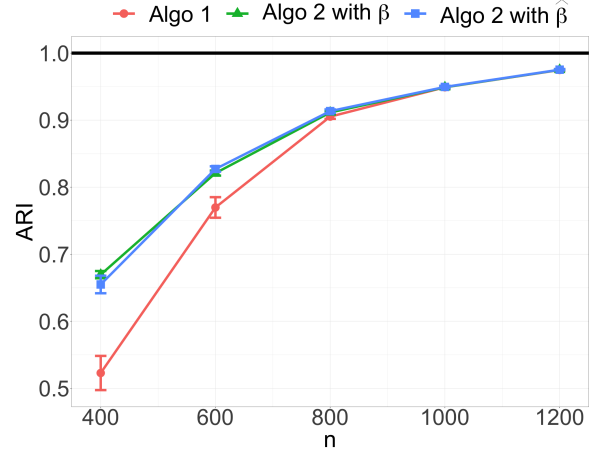
We present a comparative analysis of two model-based spectral algorithms for clustering vertices in stochastic block-model graphs with vertex covariates to assess the effect of observed and unobserved vertex heterogeneity on block

structure in graphs. The main difference of these two algorithms in estimating the induced block assignments is whether we estimate the vertex covariate effect using the observed covariate information. To analyze the algorithms' performance, we employ Chernoff information and derive the Chernoff ratio formula for homogeneous balanced model. We also simulate multiple adjacency matrices with varied type of covariates to compare the algorithms' performance via actual clustering accuracy measured by ARI. In addition, we conduct a real data analysis on a diffusion MRI connectome data set. Analytic results, simulations, and real data experiments suggest that, in general, the second algorithm is preferred: we can better estimate the induced block assignments and reveal underlying block structure by first estimating the vertex covariate effect. Our findings also emphasize the importance of distinguishing between observed and unobserved factors that can affect block structure in graphs.

We focus on the model specified as in Remark 1 where indicator function is used to measure the vertex covariate effect and identity function is used as the link between edge probabilities and latent positions. We also investigate the flexibility of our models and algorithms by considering categorical vertex covariates. The extension from discrete vertex covariates to continuous vertex covariates is under investigation, for instance, via latent structure models [35]. The indicator function is used to measure the vertex covariate effect for binary and generally categorical vertex covariates under the intuition that vertices having the same covariates are more likely to form an edge between them and different functions can be adopted for the continuous vertex covariates following the similar intuition. For example, similarity and distance functions can be chosen according to the nature of different vertex covariates to measure how they can influence graph structure. One other extension is to replace the identity link with general link function such as logit. The idea of using Chernoff information to compare algorithms' performance can be adopted for all the above generalizations and numerical



(a) ARI as β increases, {Left, Right} is treated as the induced block and {Gray, White} is treated as the vertex covariate.



(b) ARI as n increases, {Gray, White} is treated as the induced block and {Left, Right} is treated as the vertex covariate.

Fig. 7. Synthetic data analysis via a diffusion MRI connectome data set.

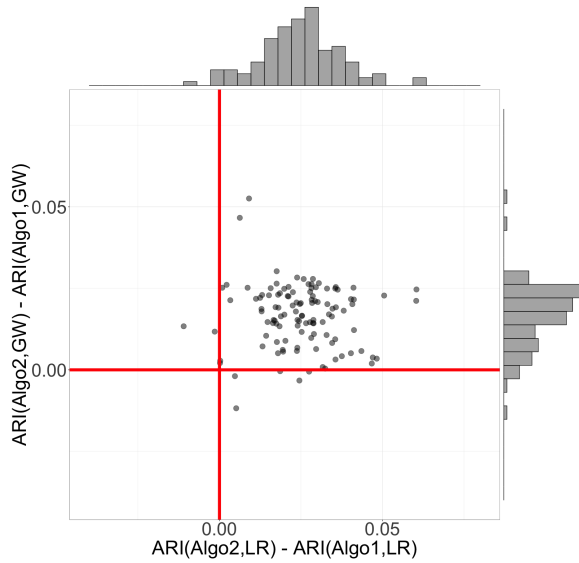


Fig. 8. Algorithms' comparative performance on connectome data via ARI.

evaluations can be obtained in the absence of closed-form expressions, which in turn can reveal how graph structure will affect our algorithms and provide guidelines for real application. Moreover, our models and algorithms can be applied to directed and bipartite graph with some modification, which is another valuable future contribution.

APPENDIX A LATENT POSITION GEOMETRY

Observe that a K -block SBM becomes a $2K$ -block SBM when adding a binary covariate that can affect block structure significantly. To analytically derive the Chernoff ratio for K -block homogeneous model with one binary covariate, we first investigate the canonical latent positions for this model via the idea of Cholesky decomposition. Specifically, let $\mathbf{B} \in [0, 1]^{K \times K}$ denote the block connectivity probability

matrix after accounting for the vertex covariate effect and $\mathbf{B}_Z \in [0, 1]^{2K \times 2K}$ denote the block connectivity probability matrix including the vertex covariate effect. Here we focus on canonical latent positions for \mathbf{B}_Z , details about the canonical latent positions for \mathbf{B} have been discussed [21]. Let $\nu_Z(K, 2K)$ denote the canonical latent position matrix, then we can re-write \mathbf{B}_Z as

$$\mathbf{B}_Z = \nu_Z(K, 2K) \nu_Z(K, 2K)^\top, \quad (41)$$

where $\nu_Z(K, 2K) = [\nu_1 \ \cdots \ \nu_{2K}]^\top$. For $K = 2$ we have via the idea of Cholesky decomposition

$$\nu_Z(2, 4) = \begin{bmatrix} \sqrt{a+\beta} & 0 & 0 \\ \frac{a}{\sqrt{a+\beta}} & \sqrt{\frac{\beta(2a+\beta)}{a+\beta}} & 0 \\ \frac{b+\beta}{\sqrt{a+\beta}} & \sqrt{\frac{\beta(b-a)^2}{(a+\beta)(2a+\beta)}} & \sqrt{\frac{2(a-b)(a+b+\beta)}{(2a+\beta)}} \\ \frac{b}{\sqrt{a+\beta}} & \sqrt{\frac{\beta(a+b+\beta)^2}{(a+\beta)(2a+\beta)}} & \sqrt{\frac{2(a-b)(a+b+\beta)}{(2a+\beta)}} \end{bmatrix}. \quad (42)$$

And by induction, for $K \geq 3$ we have

$$\begin{aligned} \nu_Z(K, 2K)_{:,1} &= \begin{bmatrix} \nu_Z(K-1, 2K-2)_{:,1:(K-1)} \\ \nu_Z(K-1, 2K-2)_{2K-3,1:(K-1)} \\ \nu_Z(K-1, 2K-2)_{2K-2,1:(K-1)} \end{bmatrix}, \\ \nu_Z(K, 2K)_{:,2} &= \begin{bmatrix} \nu_Z(K-1, 2K-2)_{:,K} \\ \kappa \nu_Z(K-1, 2K-2)_{2K-3,K} \\ \kappa \nu_Z(K-1, 2K-2)_{2K-2,K} \end{bmatrix}, \quad (43) \\ \nu_Z(K, 2K)_{:,3} &= \begin{bmatrix} \mathbf{0} \\ \sqrt{\frac{(a-b)[2a+2(K-1)b+K\beta]}{2a+2(K-2)b+(K-1)\beta}} \\ \sqrt{\frac{(a-b)[2a+2(K-1)b+K\beta]}{2a+2(K-2)b+(K-1)\beta}} \end{bmatrix}, \end{aligned}$$

where

$$\kappa = \frac{2b + \beta}{2a + 2(K-2)b + (K-1)\beta}. \quad (44)$$

For this K -block homogeneous model with one binary covariate, the symmetric structure of \mathbf{B}_Z yields

$$\begin{aligned} \boldsymbol{\nu}_1^\top \boldsymbol{\nu}_1 &= \boldsymbol{\nu}_2^\top \boldsymbol{\nu}_2 = \cdots = \boldsymbol{\nu}_{2K}^\top \boldsymbol{\nu}_{2K} = a + \beta, \\ \boldsymbol{\nu}_1^\top \boldsymbol{\nu}_2 &= \boldsymbol{\nu}_3^\top \boldsymbol{\nu}_4 = \cdots = \boldsymbol{\nu}_{2K-1}^\top \boldsymbol{\nu}_{2K} = a, \\ \boldsymbol{\nu}_1^\top \boldsymbol{\nu}_3 &= \boldsymbol{\nu}_1^\top \boldsymbol{\nu}_5 = \cdots = \boldsymbol{\nu}_{2K-2}^\top \boldsymbol{\nu}_{2K} = b + \beta, \\ \boldsymbol{\nu}_1^\top \boldsymbol{\nu}_4 &= \boldsymbol{\nu}_1^\top \boldsymbol{\nu}_6 = \cdots = \boldsymbol{\nu}_{2K-2}^\top \boldsymbol{\nu}_{2K-1} = b. \end{aligned} \quad (45)$$

Along with the balanced assumption, i.e. $\boldsymbol{\pi}_Z = (\frac{1}{2K}, \dots, \frac{1}{2K})$, the first four rows of $\boldsymbol{\nu}_Z(K, 2K)$ are ideal for derivation as they have the fewest non-zero entries and can represent all the possible geometric structure. In other word, we can only evaluate C_{12}, C_{13}, C_{14} where C_{kl} is defined as in Eq. (20) to derive the Chernoff ratio.

APPENDIX B ANALYTIC DERIVATIONS OF CHERNOFF RATIO

For K -block homogeneous model with one binary covariate, we observe that \mathbf{B}_Z has eigenvalue 0 with algebraic multiplicity $K-1$, eigenvalue $K\beta$ with algebraic multiplicity 1, eigenvalue $2(a-b)$ with algebraic multiplicity $K-1$ and eigenvalue $2a+2(K-1)b+K\beta$ with algebraic multiplicity 1. Along with the assumption that $0 < b < a < 1$ and $0 < \beta < 1$, we have among non-zero eigenvalues of \mathbf{B}_Z

$$\begin{aligned} \lambda_{\max}(\mathbf{B}_Z) &= 2a + 2(K-1)b + K\beta, \\ \lambda_{\min}(\mathbf{B}_Z) &= \begin{cases} K\beta & \text{if } \beta \leq \frac{2(a-b)}{K} \\ 2(a-b) & \text{if } \beta > \frac{2(a-b)}{K} \end{cases}. \end{aligned} \quad (46)$$

Thus \mathbf{B}_Z is positive semidefinite with $\text{rank}(\mathbf{B}_Z) = K+1$. Then we have $\mathbf{I}_{d_+, d_-} = \mathbf{I}_{K+1}$ and we can omit it in the derivations. As discussed in the previous section, we only consider the first four rows of the canonical latent position matrix $\boldsymbol{\nu}_Z(K, 2K)$ and evaluate C_{12}, C_{13}, C_{14} . With the definition as in Eq. (16), we have

$$\begin{aligned} \mathbb{E} \left[g_{\frac{1}{2}}(\boldsymbol{\nu}_1, \boldsymbol{\nu}_2, \boldsymbol{\nu}) \boldsymbol{\nu} \boldsymbol{\nu}^\top \right] &= c_0 \boldsymbol{\Delta} + c_{12} \mathbf{N}_{12} \mathbf{N}_{12}^\top, \\ \mathbb{E} \left[g_{\frac{1}{2}}(\boldsymbol{\nu}_1, \boldsymbol{\nu}_3, \boldsymbol{\nu}) \boldsymbol{\nu} \boldsymbol{\nu}^\top \right] &= \boldsymbol{\Delta}_T + c_{13} \mathbf{N}_{13} \mathbf{N}_{13}^\top + c_{24} \mathbf{N}_{24} \mathbf{N}_{24}^\top, \\ \mathbb{E} \left[g_{\frac{1}{2}}(\boldsymbol{\nu}_1, \boldsymbol{\nu}_4, \boldsymbol{\nu}) \boldsymbol{\nu} \boldsymbol{\nu}^\top \right] &= c_0 \boldsymbol{\Delta} + c_{14} \mathbf{N}_{14} \mathbf{N}_{14}^\top + c_{23} \mathbf{N}_{23} \mathbf{N}_{23}^\top, \end{aligned} \quad (47)$$

where $\boldsymbol{\Delta} \in \mathbb{R}^{(K+1) \times (K+1)}$ is defined as in Eq. (9), $\boldsymbol{\nu}_Z \in \mathbb{R}^{2K \times (K+1)}$ is defined as in Eq. (43) and

$$\begin{aligned} \phi_a &= a(1-a), \\ \phi_b &= b(1-b), \\ \phi_{b\beta} &= (b+\beta)(1-b-\beta), \\ c_0 &= \frac{\phi_b + \phi_{b\beta}}{2}, \\ c_{12} &= \frac{(a-b)(1-a-b-\beta)}{2K}, \\ c_{13} = c_{14} &= \frac{(a-b)(1-a-b-2\beta)}{4K}, \\ c_{23} = c_{24} &= \frac{\phi_a - \phi_b}{4K}, \\ c_T &= \frac{\beta(1-2b-\beta)}{4K}, \\ \mathbf{N}_{k\ell} &= [\boldsymbol{\nu}_k \quad \boldsymbol{\nu}_\ell] \in \mathbb{R}^{(K+1) \times 2}, \\ \mathbf{I}_T &= \text{diag}(1, -1, \dots, 1, -1) \in \mathbb{R}^{2K \times 2K} \\ \boldsymbol{\Delta}_T &= \boldsymbol{\nu}_Z^\top \left(c_T \mathbf{I}_T + \frac{c_0}{2K} \mathbf{I}_{2K} \right) \boldsymbol{\nu}_Z \in \mathbb{R}^{(K+1) \times (K+1)}. \end{aligned} \quad (48)$$

With the canonical latent position matrix $\boldsymbol{\nu}_Z(K, 2K)$ as in Eq. (43), observe that

$$\begin{aligned} \mathbf{N}_{12}^\top \boldsymbol{\Delta}^{-1} \mathbf{N}_{12} &= \begin{bmatrix} K+1 & K-1 \\ K-1 & K+1 \end{bmatrix}, \\ \mathbf{N}_{13}^\top \boldsymbol{\Delta}^{-1} \mathbf{N}_{13} &= \begin{bmatrix} K+1 & 1 \\ 1 & K+1 \end{bmatrix}, \\ \mathbf{N}_{14}^\top \boldsymbol{\Delta}^{-1} \mathbf{N}_{14} &= \begin{bmatrix} K+1 & -1 \\ -1 & K+1 \end{bmatrix}, \\ \mathbf{N}_{13}^\top \boldsymbol{\Delta}^{-1} \mathbf{N}_{24} &= \begin{bmatrix} K-1 & 1 \\ 1 & K-1 \end{bmatrix}, \\ \mathbf{N}_{13}^\top \boldsymbol{\Delta}_T^{-1} \mathbf{N}_{13} &= \frac{2}{n_{13}} \begin{bmatrix} \phi_b + K\phi_{b\beta} & \phi_b \\ \phi_b & \phi_b + K\phi_{b\beta} \end{bmatrix}, \\ \mathbf{N}_{24}^\top \boldsymbol{\Delta}_T^{-1} \mathbf{N}_{24} &= \frac{2}{n_{24}} \begin{bmatrix} K\phi_b + \phi_{b\beta} & \phi_{b\beta} \\ \phi_{b\beta} & K\phi_b + \phi_{b\beta} \end{bmatrix}, \\ \mathbf{N}_{13}^\top \boldsymbol{\Delta}_T^{-1} \mathbf{N}_{24} &= \frac{1}{c_0} \begin{bmatrix} K-1 & -1 \\ -1 & K-1 \end{bmatrix}, \end{aligned} \quad (49)$$

where $c_0, \phi_b, \phi_{b\beta}$ are defined as in Eq. (48) and

$$\begin{aligned} n_{13} &= 2\phi_b^2 + \beta^2(1-\beta)^2 + 3\beta\phi_b(1-2b-\beta) \\ &\quad - 4b\beta^2(1-b-\beta), \\ n_{24} &= \phi_b(\phi_b + \phi_{b\beta}). \end{aligned} \quad (50)$$

By the Sherman-Morrison-Woodbury formula [36], we have

$$\begin{aligned}
\mathbb{E} \left[g_{\frac{1}{2}}(\boldsymbol{\nu}_1, \boldsymbol{\nu}_2, \boldsymbol{\nu}) \boldsymbol{\nu} \boldsymbol{\nu}^\top \right]^{-1} &= \frac{1}{c_0} \boldsymbol{\Delta}^{-1} - \frac{1}{c_0^2} \boldsymbol{\Delta}^{-1} \mathbf{M}_{12} \boldsymbol{\Delta}^{-1}, \\
\mathbb{E} \left[g_{\frac{1}{2}}(\boldsymbol{\nu}_1, \boldsymbol{\nu}_3, \boldsymbol{\nu}) \boldsymbol{\nu} \boldsymbol{\nu}^\top \right]^{-1} &= \boldsymbol{\Delta}_T^{-1} - \boldsymbol{\Delta}_T^{-1} \mathbf{M}_{13} \boldsymbol{\Delta}_T^{-1} \\
&\quad - \boldsymbol{\Delta}_T^{-1} \mathbf{M}_{24} \boldsymbol{\Delta}_T^{-1} \\
&\quad + \boldsymbol{\Delta}_T^{-1} \mathbf{M}_{24} \boldsymbol{\Delta}_T^{-1} \mathbf{M}_{13} \boldsymbol{\Delta}_T^{-1} \\
&\quad + \boldsymbol{\Delta}_T^{-1} \mathbf{M}_{13} \boldsymbol{\Delta}_T^{-1} \mathbf{M}_{24} \boldsymbol{\Delta}_T^{-1} \\
&\quad - \boldsymbol{\Delta}_T^{-1} \mathbf{M}_{13} \boldsymbol{\Delta}_T^{-1} \mathbf{M}_{24} \\
&\quad \quad \boldsymbol{\Delta}_T^{-1} \mathbf{M}_{13} \boldsymbol{\Delta}_T^{-1}, \\
\mathbb{E} \left[g_{\frac{1}{2}}(\boldsymbol{\nu}_1, \boldsymbol{\nu}_4, \boldsymbol{\nu}) \boldsymbol{\nu} \boldsymbol{\nu}^\top \right]^{-1} &= \frac{1}{c_0} \boldsymbol{\Delta}^{-1} - \frac{1}{c_0^2} \boldsymbol{\Delta}^{-1} \mathbf{M}_{14} \boldsymbol{\Delta}^{-1} \\
&\quad - \frac{1}{c_0^2} \boldsymbol{\Delta}^{-1} \mathbf{M}_{23} \boldsymbol{\Delta}^{-1} \\
&\quad + \frac{1}{c_0^3} \boldsymbol{\Delta}^{-1} \mathbf{M}_{23} \boldsymbol{\Delta}^{-1} \mathbf{M}_{14} \boldsymbol{\Delta}^{-1} \\
&\quad + \frac{1}{c_0^3} \boldsymbol{\Delta}^{-1} \mathbf{M}_{14} \boldsymbol{\Delta}^{-1} \mathbf{M}_{23} \boldsymbol{\Delta}^{-1} \\
&\quad - \frac{1}{c_0^4} \boldsymbol{\Delta}^{-1} \mathbf{M}_{14} \boldsymbol{\Delta}^{-1} \mathbf{M}_{23} \\
&\quad \quad \boldsymbol{\Delta}^{-1} \mathbf{M}_{14} \boldsymbol{\Delta}^{-1},
\end{aligned} \tag{51}$$

where $c_0, c_{12}, c_{13}, c_{14}, c_{23}, c_{24}$ are defined as in Eq. (48) and

$$\begin{aligned}
\mathbf{D}_{12} &= \frac{1}{c_{12}} \mathbf{I}_2 + \frac{1}{c_0} \mathbf{N}_{12}^\top \boldsymbol{\Delta}^{-1} \mathbf{N}_{12}, \\
\mathbf{D}_{13} &= \frac{1}{c_{13}} \mathbf{I}_2 + \mathbf{N}_{13}^\top \boldsymbol{\Delta}_T^{-1} \mathbf{N}_{13}, \\
\mathbf{D}_{14} &= \frac{1}{c_{14}} \mathbf{I}_2 + \frac{1}{c_0} \mathbf{N}_{14}^\top \boldsymbol{\Delta}^{-1} \mathbf{N}_{14}, \\
\mathbf{M}_{12} &= \mathbf{N}_{12} \mathbf{D}_{12}^{-1} \mathbf{N}_{12}^\top, \\
\mathbf{M}_{13} &= \mathbf{N}_{13} \mathbf{D}_{13}^{-1} \mathbf{N}_{13}^\top, \\
\mathbf{M}_{14} &= \mathbf{N}_{14} \mathbf{D}_{14}^{-1} \mathbf{N}_{14}^\top, \\
\mathbf{D}_{23} &= \frac{1}{c_{23}} \mathbf{I}_2 + \frac{1}{c_0} \mathbf{N}_{23}^\top \boldsymbol{\Delta}^{-1} \mathbf{N}_{23} \\
&\quad - \frac{1}{c_0^2} \mathbf{N}_{23}^\top \boldsymbol{\Delta}^{-1} \mathbf{M}_{14} \boldsymbol{\Delta}^{-1} \mathbf{N}_{23}, \\
\mathbf{D}_{24} &= \frac{1}{c_{24}} \mathbf{I}_2 + \mathbf{N}_{24}^\top \boldsymbol{\Delta}_T^{-1} \mathbf{N}_{24} \\
&\quad - \mathbf{N}_{24}^\top \boldsymbol{\Delta}_T^{-1} \mathbf{M}_{13} \boldsymbol{\Delta}_T^{-1} \mathbf{N}_{24}, \\
\mathbf{M}_{23} &= \mathbf{N}_{23} \mathbf{D}_{23}^{-1} \mathbf{N}_{23}^\top, \\
\mathbf{M}_{24} &= \mathbf{N}_{24} \mathbf{D}_{24}^{-1} \mathbf{N}_{24}^\top.
\end{aligned} \tag{52}$$

Again by canonical latent position matrix $\boldsymbol{\nu}_Z(K, 2K)$ as in Eq. (43), we have

$$\begin{aligned}
(\boldsymbol{\nu}_1 - \boldsymbol{\nu}_2)^\top \boldsymbol{\Delta} (\boldsymbol{\nu}_1 - \boldsymbol{\nu}_2) &= \beta^2, \\
(\boldsymbol{\nu}_1 - \boldsymbol{\nu}_3)^\top \boldsymbol{\Delta} (\boldsymbol{\nu}_1 - \boldsymbol{\nu}_3) &= \frac{2}{K} (a - b)^2, \\
(\boldsymbol{\nu}_1 - \boldsymbol{\nu}_4)^\top \boldsymbol{\Delta} (\boldsymbol{\nu}_1 - \boldsymbol{\nu}_4) &= \frac{2}{K} (a - b)^2 + \beta^2, \\
(\boldsymbol{\nu}_1 - \boldsymbol{\nu}_3)^\top \boldsymbol{\Delta} \boldsymbol{\Delta}_T^{-1} \boldsymbol{\Delta} (\boldsymbol{\nu}_1 - \boldsymbol{\nu}_3) &= \frac{1}{c_0} \frac{2}{K} (a - b)^2.
\end{aligned} \tag{53}$$

Similarly, we have

$$\begin{aligned}
\mathbf{N}_{12}^\top (\boldsymbol{\nu}_1 - \boldsymbol{\nu}_2) &= \beta [1 \quad -1]^\top, \\
\mathbf{N}_{13}^\top (\boldsymbol{\nu}_1 - \boldsymbol{\nu}_3) &= (a - b) [1 \quad -1]^\top, \\
\mathbf{N}_{14}^\top (\boldsymbol{\nu}_1 - \boldsymbol{\nu}_4) &= (a - b + \beta) [1 \quad -1]^\top, \\
\mathbf{N}_{23}^\top (\boldsymbol{\nu}_1 - \boldsymbol{\nu}_4) &= (a - b - \beta) [1 \quad -1]^\top, \\
\mathbf{N}_{13}^\top \boldsymbol{\Delta}_T^{-1} \boldsymbol{\Delta} (\boldsymbol{\nu}_1 - \boldsymbol{\nu}_3) &= \frac{(a - b)}{c_0} [1 \quad -1]^\top.
\end{aligned} \tag{54}$$

Then with all the results above, we have

$$\begin{aligned}
C_{12} &= \frac{K\beta^2}{2D_4}, \\
C_{13} &= \frac{(a - b)^2}{K(\phi_a + \phi_b + \phi_\beta)}, \\
C_{14} &= \frac{K^2\beta^2(\phi_a + \phi_b + \phi_\beta) + 2KN_3 + 4N_4}{2K[2(\phi_a^2 - \phi_b^2) + D_5]},
\end{aligned} \tag{55}$$

where ϕ_a, ϕ_b are defined as in Eq. (48) and

$$\begin{aligned}
\phi_\beta &= \beta(1 - a - b - \beta), \\
D_3 &= K - 2a - 2(K - 1)b - K\beta, \\
D_4 &= 2\phi_a + 2(K - 1)\phi_b + \beta D_3, \\
N_3 &= (a - b)^2[2\phi_b + \beta(1 + \beta - 2b)], \\
N_4 &= (a - b)^3(1 - a - b - \beta), \\
D_5 &= 2\beta(a - b)[(1 - a - b - \beta) - 2(\phi_a + \phi_b) \\
&\quad - \phi_\beta + 2b(a + \beta)] + K\{2\phi_b(\phi_a + \phi_b) \\
&\quad - 2b\beta(\phi_b + a - b^2) - 2ab\phi_\beta + \beta(1 - \beta)[\phi_a \\
&\quad + (3b + \beta)(1 - \beta) - a\beta - 5b^2]\}.
\end{aligned} \tag{56}$$

Then we have the approximate Chernoff information for Algorithm 1 as

$$\rho_1^* \approx \min_{\ell \in \{2, 3, 4\}} C_{1\ell}, \tag{57}$$

where $C_{1\ell}$ for $\ell \in \{2, 3, 4\}$ are defined as in Eq. (55). Also observe that

$$\begin{aligned}
C_{12} - C_{14} &= \frac{-(a - b)^2 N_6^2}{KD_4[2(\phi_a^2 - \phi_b^2) + D_5]}, \\
C_{13} - C_{14} &= \frac{-\beta^2[2(a - b)^2 + K(\phi_a + \phi_b + \phi_\beta)]^2}{2K(\phi_a + \phi_b + \phi_\beta)[2(\phi_a^2 - \phi_b^2) + D_5]},
\end{aligned} \tag{58}$$

where ϕ_a, ϕ_b are defined as in Eq. (48), ϕ_β, D_4, D_5 are defined as in Eq. (56) and

$$\begin{aligned} N_5 &= \beta[K - 2a - 2(K - 1)b], \\ N_6 &= 2\phi_a + 2(K - 1)\phi_b + N_5. \end{aligned} \quad (59)$$

Subsequent calculations and simplification yield ρ_1^* as in Eq. (34).

REFERENCES

- [1] E. Abbe, “Community detection and stochastic block models: recent developments,” *Journal of Machine Learning Research*, vol. 18, no. 1, pp. 6446–6531, 2017.
- [2] P. W. Holland, K. B. Laskey, and S. Leinhardt, “Stochastic blockmodels: First steps,” *Social Networks*, vol. 5, no. 2, pp. 109–137, 1983.
- [3] B. Karrer and M. E. Newman, “Stochastic blockmodels and community structure in networks,” *Physical Review E*, vol. 83, no. 1, p. 016107, 2011.
- [4] D. S. Choi, P. J. Wolfe, and E. M. Airolidi, “Stochastic blockmodels with a growing number of classes,” *Biometrika*, vol. 99, no. 2, pp. 273–284, 2012.
- [5] S. Roy, Y. Atchadé, and G. Michailidis, “Likelihood inference for large scale stochastic blockmodels with covariates based on a divide-and-conquer parallelizable algorithm with communication,” *Journal of Computational and Graphical Statistics*, vol. 28, no. 3, pp. 609–619, 2019.
- [6] T. M. Sweet, “Incorporating covariates into stochastic blockmodels,” *Journal of Educational and Behavioral Statistics*, vol. 40, no. 6, pp. 635–664, 2015.
- [7] N. Binkiewicz, J. T. Vogelstein, and K. Rohe, “Covariate-assisted spectral clustering,” *Biometrika*, vol. 104, no. 2, pp. 361–377, 2017.
- [8] S. Huang and Y. Feng, “Pairwise covariates-adjusted block model for community detection,” *arXiv preprint arXiv:1807.03469*, 2018.
- [9] A. Mele, L. Hao, J. Cape, and C. E. Priebe, “Spectral inference for large stochastic blockmodels with nodal covariates,” *arXiv preprint arXiv:1908.06438*, 2019.
- [10] U. Von Luxburg, “A tutorial on spectral clustering,” *Statistics and Computing*, vol. 17, no. 4, pp. 395–416, 2007.
- [11] V. Lyzinski, D. L. Sussman, M. Tang, A. Athreya, and C. E. Priebe, “Perfect clustering for stochastic blockmodel graphs via adjacency spectral embedding,” *Electronic Journal of Statistics*, vol. 8, no. 2, pp. 2905–2922, 2014.
- [12] V. Lyzinski, M. Tang, A. Athreya, Y. Park, and C. E. Priebe, “Community detection and classification in hierarchical stochastic blockmodels,” *IEEE Transactions on Network Science and Engineering*, vol. 4, no. 1, pp. 13–26, 2016.
- [13] F. McSherry, “Spectral partitioning of random graphs,” in *Proceedings 42nd IEEE Symposium on Foundations of Computer Science*. IEEE, 2001, pp. 529–537.
- [14] K. Rohe, S. Chatterjee, and B. Yu, “Spectral clustering and the high-dimensional stochastic blockmodel,” *The Annals of Statistics*, vol. 39, no. 4, pp. 1878–1915, 2011.
- [15] V. Lyzinski, K. Levin, and C. E. Priebe, “On consistent vertex nomination schemes,” *Journal of Machine Learning Research*, vol. 20, no. 69, pp. 1–39, 2019.
- [16] M. Tang, A. Athreya, D. L. Sussman, V. Lyzinski, and C. E. Priebe, “A nonparametric two-sample hypothesis testing problem for random graphs,” *Bernoulli*, vol. 23, no. 3, pp. 1599–1630, 2017.
- [17] S. Wang, J. Arroyo, J. T. Vogelstein, and C. E. Priebe, “Joint embedding of graphs,” *IEEE Transactions on Pattern Analysis and Machine Intelligence*, 2019.
- [18] D. L. Sussman, M. Tang, D. E. Fishkind, and C. E. Priebe, “A consistent adjacency spectral embedding for stochastic blockmodel graphs,” *Journal of the American Statistical Association*, vol. 107, no. 499, pp. 1119–1128, 2012.
- [19] A. Athreya, C. E. Priebe, M. Tang, V. Lyzinski, D. J. Marchette, and D. L. Sussman, “A limit theorem for scaled eigenvectors of random dot product graphs,” *Sankhya A*, vol. 78, no. 1, pp. 1–18, 2016.
- [20] M. Tang and C. E. Priebe, “Limit theorems for eigenvectors of the normalized laplacian for random graphs,” *The Annals of Statistics*, vol. 46, no. 5, pp. 2360–2415, 2018.
- [21] J. Cape, M. Tang, and C. E. Priebe, “On spectral embedding performance and elucidating network structure in stochastic blockmodel graphs,” *Network Science*, vol. 7, no. 3, pp. 269–291, 2019.
- [22] L. Hao, A. Mele, J. Cape, A. Athreya, C. Mu, and C. E. Priebe, “Latent communities in employment relation and wage distribution: a network approach,” *submitted*, 2020.
- [23] C. R. Shalizi and E. McFowland III, “Estimating causal peer influence in homophilous social networks by inferring latent locations,” *arXiv preprint arXiv:1607.06565*, 2016.
- [24] P. D. Hoff, A. E. Raftery, and M. S. Handcock, “Latent space approaches to social network analysis,” *Journal of the American Statistical Association*, vol. 97, no. 460, pp. 1090–1098, 2002.
- [25] M. S. Handcock, A. E. Raftery, and J. M. Tantrum, “Model-based clustering for social networks,” *Journal of the Royal Statistical Society: Series A (Statistics in Society)*, vol. 170, no. 2, pp. 301–354, 2007.
- [26] P. Rubin-Delanchy, C. E. Priebe, M. Tang, and J. Cape, “A statistical interpretation of spectral embedding: the generalised random dot product graph,” *arXiv preprint arXiv:1709.05506*, 2017.
- [27] T. Hastie, R. Tibshirani, and J. Friedman, *The Elements of Statistical Learning: Data Mining, Inference, and Prediction*. Springer Science & Business Media, 2009.
- [28] I. T. Jolliffe and J. Cadima, “Principal component analysis: a review and recent developments,” *Philosophical Transactions of the Royal Society A: Mathematical, Physical and Engineering Sciences*, vol. 374, no. 2065, p. 20150202, 2016.
- [29] M. Zhu and A. Ghodsi, “Automatic dimensionality selection from the scree plot via the use of profile likelihood,” *Computational Statistics & Data Analysis*, vol. 51, no. 2, pp. 918–930, 2006.
- [30] A. Athreya, D. E. Fishkind, M. Tang, C. E. Priebe, Y. Park, J. T. Vogelstein, K. Levin, V. Lyzinski, and Y. Qin, “Statistical inference on random dot product graphs: a survey,” *Journal of Machine Learning Research*, vol. 18, no. 1, pp. 8393–8484, 2017.
- [31] H. Chernoff, “A measure of asymptotic efficiency for tests of a hypothesis based on the sum of observations,” *The Annals of Mathematical Statistics*, vol. 23, no. 4, pp. 493–507, 1952.
- [32] —, “Large-sample theory: Parametric case,” *The Annals of Mathematical Statistics*, vol. 27, no. 1, pp. 1–22, 1956.
- [33] C. E. Priebe, Y. Park, J. T. Vogelstein, J. M. Conroy, V. Lyzinski, M. Tang, A. Athreya, J. Cape, and E. Bridgeford, “On a two-truths phenomenon in spectral graph clustering,” *Proceedings of the National Academy of Sciences*, vol. 116, no. 13, pp. 5995–6000, 2019.
- [34] G. Kiar, E. W. Bridgeford, W. R. Gray Roncal, V. Chandrashekar, D. Mhembe, S. Ryman, X.-N. Zuo, D. S. Margulies, R. C. Craddock, C. E. Priebe, R. Jung, V. D. Calhoun, B. Caffo, R. Burns, M. P. Milham, and J. T. Vogelstein, “A high-throughput pipeline identifies robust connectomes but troublesome variability,” *bioRxiv*, p. 188706, 2018.
- [35] A. Athreya, M. Tang, Y. Park, and C. E. Priebe, “On estimation and inference in latent structure random graphs,” *Statistical Science*, vol. accepted for publication, 2020.
- [36] R. A. Horn and C. R. Johnson, *Matrix Analysis*. Cambridge university press, 2012.